Improving Process Level Understanding of Boundary Layer Winds over the Northeast U.S. Shelf: The Third Wind Forecast Improvement Project (WFIP3)

A. Kirincich[a] , R. Krishnamurthy[b] , D.D. Turner[c] , B. Adler[d,e] , N. Agarwal[f,g] , L. K. Berg [b] , L. Bianco[d,e] , N. Bodini[h] , M. Chabert d'Hieres[i] , J. T. Farrar[a] , H.J.S. Fernando[i] , B. Gaudet[b] , V. P. Ghate[j] , L. Goldberger[b] , A. O. Gonzalez[a] , E. Hall[k] , E. Hines[q] , G. Hodges[d,k] , G. V. Iungo[l] , R. Jackson[j] , H. Jiang[a] , A. Kinsella [a] , B. Kosovic[f] , R. Kotamarthi[j] , S Letizia[h] , S. Lipari[b] , J. K. Lundquist[f,g,h] , J. Mirocha[m] , C. Moss[l] , P. Muradyan[j] , T. Myers[r] , R.K. Newsom[b] , J. O'Brien[j] , J.B. Olson[c] , M. Pekour[b] , M. Puccioni[m] , D. Rosencrans[g] , S. Roy[l] , C. Sauvage[a,n] , J. Sedlar[d,k] , H. Seo[a,n] , M. Shams Solari[l] , L. Soldo[d,k] , S. Stierle[d,k] , X. Sun[c,d] , E. J. Thompson[e] , E. Traiger[o] , S. Wharton[m] , J. Wilczak[e] , S. Zippel[a,p]

[a] *Woods Hole Oceanographic Institution, Woods Hole, MA, USA;* [b] *Pacific Northwest National Laboratory, Richland, WA, USA;* [c] *Global Systems Laboratory, National Oceanic and Atmospheric Administration, Boulder, CO, USA;* [d] *Cooperative Institute for Research in Environmental Sciences, University of Colorado Boulder, Boulder, CO, USA,* [e] *Physical Sciences Laboratory, National Oceanic and Atmospheric Administration, Boulder, CO, USA,* [f] *Johns Hopkins University, USA,* [g] *University of Colorado, Boulder, CO, USA,* [h] *National Laboratory of the Rockies, Golden, CO, USA,* [i] *Notre Dame University, IN, USA,* [j] *Argonne National Laboratory, Chicago, IL, USA,* [k] *Global Monitoring Laboratory, National Oceanic and Atmospheric Administration, Boulder, CO, USA,* [l] *University of Texas at Dallas, Dallas, TX, USA,* [m] *Lawrence Livermore National Laboratory, CA, USA,* [n] *University of Hawai'i, Mānoa, Honolulu, HI, USA,* [o] *DNV USA, Boston, MA, USA;* [p] *Oregon State University, Corvallis, OR, USA;* [q] *Tufts University, Boston, MA, USA* [r] *Department of Atmospheric Science, University of Wyoming, Laramie, WY, USA*

Corresponding author: Anthony Kirincich, akirincich@whoi.edu

Early Online Release: This preliminary version has been accepted for publication in *Bulletin of the American Meteorological Society*, may be fully cited, and has been assigned DOI 10.1175/BAMS-D-25-0201.1. The final typeset copyedited article will replace the EOR at the above DOI when it is published.

ABSTRACT: The third Wind Forecast Improvement Project (WFIP3), a U.S. Department of Energy and National Oceanic and Atmospheric Administration sponsored investigation, sought to improve understanding of the physical phenomena in the atmosphere and ocean that dictate the structure and variability of wind and thermodynamic fields within the marine atmospheric boundary layer. WFIP3 focused on mesoscale and submesoscale flows – including sea breezes, low-level jets, low-level clouds, and coastal storms – and the ability of advanced numerical model parameterizations to represent them within fully coupled oceanic and atmospheric modeling systems and foundational weather forecast models. WFIP3 conducted a comprehensive 18-month observational study over the Northeast U.S. outer continental shelf, a high-use coastal zone, using a 3D multiscale sensor array to highly resolve the temporal, vertical, and horizontal structure of the coupled atmospheric and oceanic boundary layers. Multiple land-based study sites adjacent to the coastal ocean observed surface meteorology and vertical profiles of atmospheric properties via passive infrared and microwave radiometers, active lidars and radars, and radiosondes. At sea, an array of surface flux buoys and two vertical profiling lidar buoys observed both atmospheric and oceanic properties, augmented by land-based oceanographic radar systems and routine ship-based surveys. Intensive observations of the marine atmospheric boundary layer over the ocean was done from an air-sea interaction flux tower and extended deployments of a large autonomous barge platform. Numerous critical forecasting phenomena were observed that are being evaluated within regional coupled and uncoupled modeling systems, including the National Oceanic and Atmospheric Administration's foundational High-Resolution Rapid Refresh forecast model.

Accepted for publication in *Bulletin of the American Meteorological Society.* DOI 10.1175/BAMS-D-25-0201.1.

SIGNIFICANCE STATEMENT: As the first Wind Forecast Improvement Project (WFIP) focused on the coastal and nearshore environment, the third WFIP, called WFIP3, is a critical step in our collective efforts to understand the structure and variability of wind and thermodynamic fields within the marine atmospheric boundary layer and how it is represented within numerical weather models. The large field program, conducted between November 2023 and August 2025, involved numerous research institutions, four national labs of the U.S. Department of Energy, and three National Oceanic and Atmospheric Administration research labs.

CAPSULE: Focused on coastal areas, WFIP3 provides a detailed look at vertical structure and horizontal variability of the marine atmospheric boundary layer and its representation within numerical weather models.

1. Introduction

The marine atmospheric boundary layer (MABL) plays a critical role in regulating the exchange of momentum, heat, and moisture between the atmosphere and ocean at various spatial and temporal scales. It is a highly dynamic system influenced by atmospheric stability, mesoscale weather phenomena, ocean surface conditions (e.g., sea surface temperatures (SSTs), waves, and currents), and moist processes such as cloud formation and precipitation (Edson et al. 2007; Clayson et al. 2023). The unique characteristics of the MABL, including its spatial and temporal variability, strongly impact the development of winds, turbulence, stratification, and marine cloud patterns that propagate through the atmosphere and affect both global- and regional-scale atmospheric circulation. The ability to accurately forecast such phenomena is a grand challenge in atmospheric sciences (National Research Council 2018; Shaw et al. 2022; Brotzge et al. 2023).

Understanding the processes governing the MABL requires an integrative approach that combines state-of-art field observations, modeling, and theoretical analysis. Previous studies have shown that the depth of the MABL varies significantly due to atmospheric thermodynamic conditions, surface heat fluxes, and mesoscale phenomena such as gravity waves, low-level jets (LLJs), and land-sea breeze circulations (e.g., Archer et al. 2016; Wenegrat and Arthur 2018; Piazza et al. 2016). These variations have a profound effect on turbulent eddies, surface layer dynamics, and internal boundary layer formation (e.g., Stull 1988). Furthermore, moist processes such as latent

Accepted for publication in *Bulletin of the American Meteorological Society.* DOI 10.1175/BAMS-D-25-0201.1.

heat fluxes and interactions with low-level clouds play an essential role in modulating the vertical thermodynamic structure of the MABL, buoyancy fluxes, and turbulence budgets (Wood 2012).

At the air-sea interface, interactions between the atmosphere and ocean are highly influenced by factors such as SST gradients, waves and wind-wave coupling, and ocean currents. These processes regulate the vertical transfer of momentum and energy, leading to significant variability in the MABL depth and turbulence intensity based on atmospheric stability and mesoscale forcing (e.g., Nonaka and Xie 2003; Sullivan et al. 2008, 2025). Although progress has been made in understanding ocean-atmosphere interactions, the absence of detailed observations over the ocean significantly impedes advancements in understanding and parameterizing these interactions in modern numerical weather models (Clayson et al. 2023). Observations within the air-sea transition zone across a range of scales are essential for improvement and verification of coupled prediction models.

The third Wind Forecast Improvement Project (WFIP3), organized and funded by the U.S. Department of Energy (DOE) and the National Oceanic and Atmospheric Administration (NOAA), sought to advance understanding of the structure and variability of the MABL and how it is represented within numerical weather models. Previous wind forecast improvement efforts have been conducted across the Midwest and central plains (WFIP1: Wilczak et al. 2015), as well as the Columbia River Basin region in the U.S. Pacific Northwest (WFIP2: Shaw et al. 2019). WFIP3 is the first WFIP focused on the coastal oceanic environment. It involved numerous research institutions, including four DOE national labs, three NOAA research labs, two NOAA weather forecasting offices, and multiple universities and private companies (Table 1). With field observations conducted between November 2023 and August 2025, we describe the project's focus, the scope of the field campaign, preliminary results, and the datasets available for future research studies.

WFIP3 was carried out on the U.S. East Coast (Fig. 1), as it is both a high-use coastal zone and exhibits strong seasonality in atmospheric and oceanic properties at a range of scales (Sorooshian et al. 2020; Lentz 2008; Wang et al. 2018; Shutt and Seim 2020). In the region, seasonal- and event-scale variations in air and water temperatures, atmospheric stability, storm tracks, and oceanic mixed layer depths drive a dynamic coastal zone (e.g. Lombardo and Kading 2018). LLJs, a key atmospheric boundary layer phenomena, are ubiquitous in the region, as demonstrated by prior

Accepted for publication in *Bulletin of the American Meteorological Society.* DOI 10.1175/BAMS-D-25-0201.1.

Table 1. WFIP3 Project Team

Non-Federal Team	DOE National Labs	NOAA	User Advisory Board
Woods Hole Oceanographic Institution (WHOI)	Pacific Northwest National Laboratory (PNNL)	Global Systems Lab	ISO New England
University of Colorado Boulder	National Laboratory of the Rockies	Physical Sciences Lab	Equinor
University of Texas at Dallas	Lawrence Livermore National Laboratory	Global Monitoring Lab	Vineyard Wind
Oregon State University	Argonne National Laboratory	WFO** Boston	Avangrid
University of Hawaii		WFO Upton	U.S. Coast Guard
Tufts University			Orsted
Johns Hopkins University			Regional Wildlife Science Collaborative
University of Notre Dame*			
DNV USA			

*contributed via a subcontract to PNNL
**WFO – National Weather Service Weather Forecast Office

studies (Archer et al. 2016; Pichugina et al. 2017; Debnath et al. 2021; Aird et al. 2022; de Jong et al. 2023; Quint et al. 2025). The project focused on the Northeast Shelf to take advantage of existing observational assets, including numerous land-based instrumented sites proximate to the coastal zone and an offshore fixed tower. These assets allowed the project to address key research topics, including the vertical structure of momentum flux in atmospheric and oceanic surface layers, parameterizations of boundary layer clouds, moist convective and precipitation processes, and the linkages of these topics to changes in ocean surface conditions and coastal weather phenomena such as squall lines, marine fog, cold-air outbreaks, and winter storms.

This paper presents the overarching scientific justification for the WFIP3 project and describes the recently completed field observational campaign. Scientific background for the project's efforts and its goals are presented first, followed by a detailed description of the field program. Project data products and data access are presented next, followed by results of the preliminary analyses, their implications, and conclusions.

2. Scientific Background

a. Prior Work

WFIP1 and WFIP2 demonstrated that major advances are possible in our ability to model low-level winds and turbulence of consequence to weather forecasting through a combination of

Accepted for publication in *Bulletin of the American Meteorological Society.* DOI 10.1175/BAMS-D-25-0201.1.

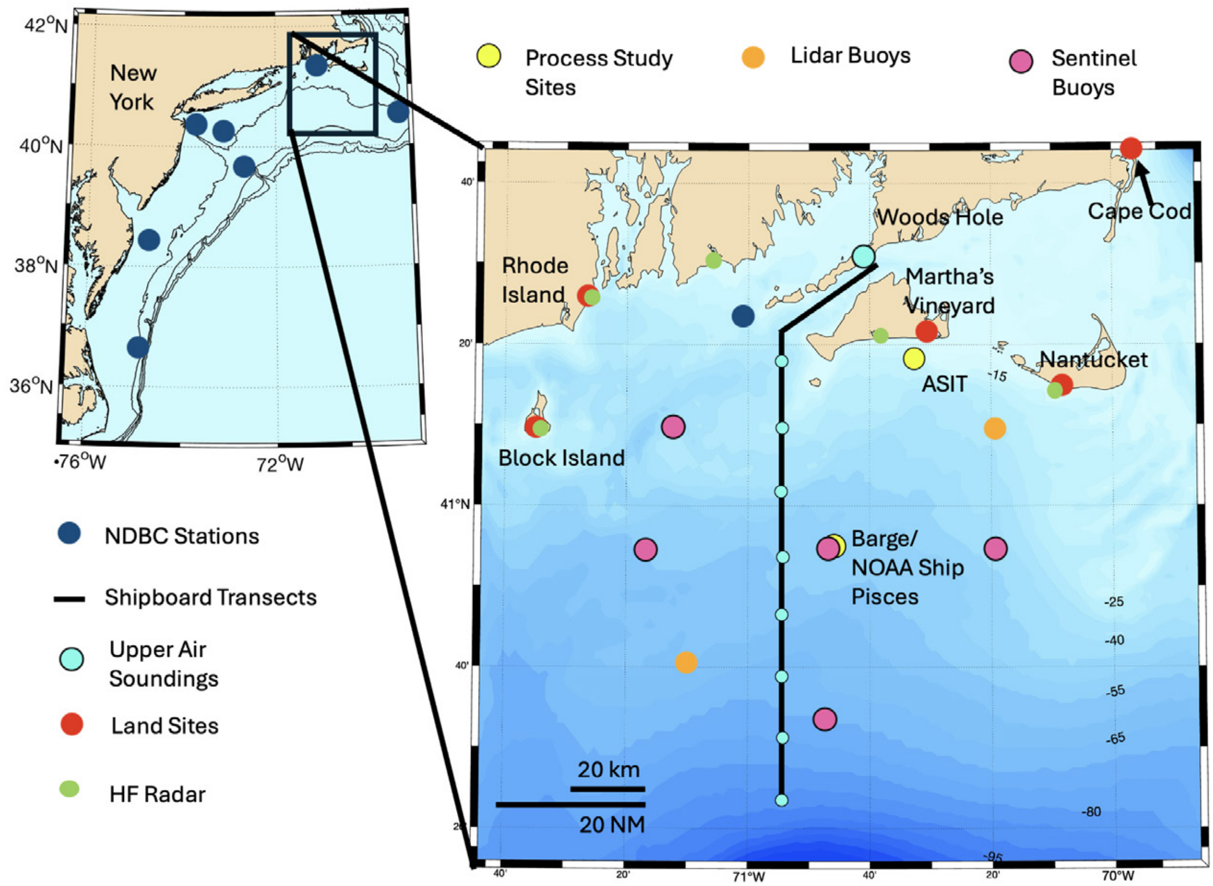

FIG. 1. The Northeast Shelf of the U.S. East Coast (inset) covering the Rhode Island and Massachusetts coastal regions. The WFIP3 land and ocean field site locations are labeled by their activity along with long term High Frequency (HF) Radar installations and National Data Buoy Center (NDBC) buoy locations.

observational, theoretical, and numerical advances. These efforts (i.e. Wilczak et al. 2015, 2019; Shaw et al. 2019; Olson et al. 2019b) carried out comprehensive field observations and utilized the results to validate both regional and operational weather prediction models. Just as on land, there are substantial, unsolved problems in forecasting winds and turbulence over the coastal ocean (National Research Council 1997; Archer et al. 2016; Bourassa et al. 2019), and the uncertainties that result are critical for maritime operations, search and rescue, and aviation forecasts, as well as for energy usage forecasts on regional scales.

WFIP3 was informed by a community workshop convened by DOE in 2019 (Shaw et al. 2022), which sought to identify the key scientific challenges in characterizing the marine atmosphere.

Accepted for publication in *Bulletin of the American Meteorological Society.* DOI 10.1175/BAMS-D-25-0201.1.

Shaw et al. (2022) and subsequent efforts among the assembled WFIP3 team identified key focus areas and research needs that informed the project's observational efforts, including:

- Understanding the characteristics of the atmospheric surface layer over the ocean and advancing surface layer parameterizations,

- Measuring wind shear, veer, and turbulence within the MABL in order to validate numerical models,

- Resolving atmospheric stability within the MABL and improving modeling of vertical fluxes in a stratified MABL,

- Uncovering feedback between atmospheric and oceanic mesoscale and submesoscale flows and their impacts on synoptic and regional forecast accuracies.

Previous efforts focused on air-sea interactions and fluxes over the ocean have improved our knowledge of coupled boundary layer processes and the parameterization of fluxes (e.g., the COARE flux algorithm: Fairall et al. 2003; Edson et al. 2013) that set the structure and depth of the surface layer. Surface waves are a critical contributor to momentum flux at the air-sea interface, and updates to COARE have sought to improve representation of their impact on fluxes. Form drag, which arises from coherent pressure patterns over surface waves, is widely regarded as a dominant mechanism determining air-sea fluxes and can drive sizable variability in exchange coefficients across different sea states at similar wind speeds. The connection between the friction velocity (u_*) and turbulent fluxes of heat and moisture highlights the importance of wind-wave interactions for all turbulent exchanges at the interface and the wave-related surface processes that govern air-sea exchange. These processes are particularly significant under high-wind conditions and during extreme events, where traditional parameterizations often fail to reduce prediction biases (Bidlot and Janssen 2024). While these improvements in air-sea interaction parameterizations have been incorporated into oceanic models and process studies, their inclusion into the over-ocean component of atmospheric mesoscale models has not kept pace. Additionally, recent land-based studies using the Weather Research and Forecasting (WRF) model over complex terrain (e.g. Olson et al. 2019b; Kosović et al. 2020; Juliano et al. 2022) have developed new boundary layer parameterizations that may be well suited for the heterogeneity of coastal regions.

Accepted for publication in *Bulletin of the American Meteorological Society.* DOI 10.1175/BAMS-D-25-0201.1.

Previous efforts in the region have examined the impacts of stability over the marine atmosphere on characterizing atmospheric processes. For example, Bodini et al. (2019a) found exceedingly low levels of atmospheric turbulence over the ocean during the onshore wind conditions that frequently occur during stably stratified periods (Fig. 2). Jiang and Edson (2020) found the best agreement between WRF and offshore lidar observations during convective conditions, with WRF consistently underestimating LLJs, near-surface shear, veer, and turbulence of atmospheric winds in stably stratified conditions when flows are dictated by interactions with the water surface and overlying stratification. At the ocean's surface, Kirincich et al. (2022) documented the extent of strong and persistent oceanic SST gradients in the region and their impact on ocean currents at oceanic mesoscales and submesoscales (Fig. 3). The impact of mesoscale SST variability on the generation of low-level clouds and marine fog, a critical feature of the study area, is poorly represented within models. Shaw et al. (2022) and others have hypothesized that 3D planetary boundary layer (PBL) schemes as well as coupled ocean-wave-atmospheric models (i.e., Kosović et al. 2020; Juliano et al. 2022; Sauvage et al. 2023) are required to increase forecast fidelity for these features as well as the patchiness of precipitation events that depend on the land-sea gradients or oceanic surface properties. Thus, the central hypothesis of WFIP3 is that variability in the properties of the coastal ocean will impact the winds and atmospheric stability within the air-sea transition zone (upper ocean, air-sea interface, and atmospheric marine boundary layer).

b. Study Area

WFIP3 was conducted in the northeastern third of the Mid-Atlantic Bight, a high-traffic marine area with large adjacent population centers (Fig. 1). The area features a relatively wide shelf bordered by the Gulf Stream offshore and the continental landmass to the north. Atmospheric conditions are dominated by a seasonal shift in wind patterns from southwesterly winds during warmer, more stratified summer months to cold, dry northwesterly winds during winter months (Fig. 2). Oceanic conditions include a dramatic (15°C) seasonal cycle in water temperatures and continuous ocean heat export due to a predominant westward flow of shelf waters from the cold water sources of the Gulf of Maine southwestward along the shelf. However, sharp temperature features at the ocean's surface vary on synoptic timescales and, due to their contribution to

Accepted for publication in *Bulletin of the American Meteorological Society.* DOI 10.1175/BAMS-D-25-0201.1.

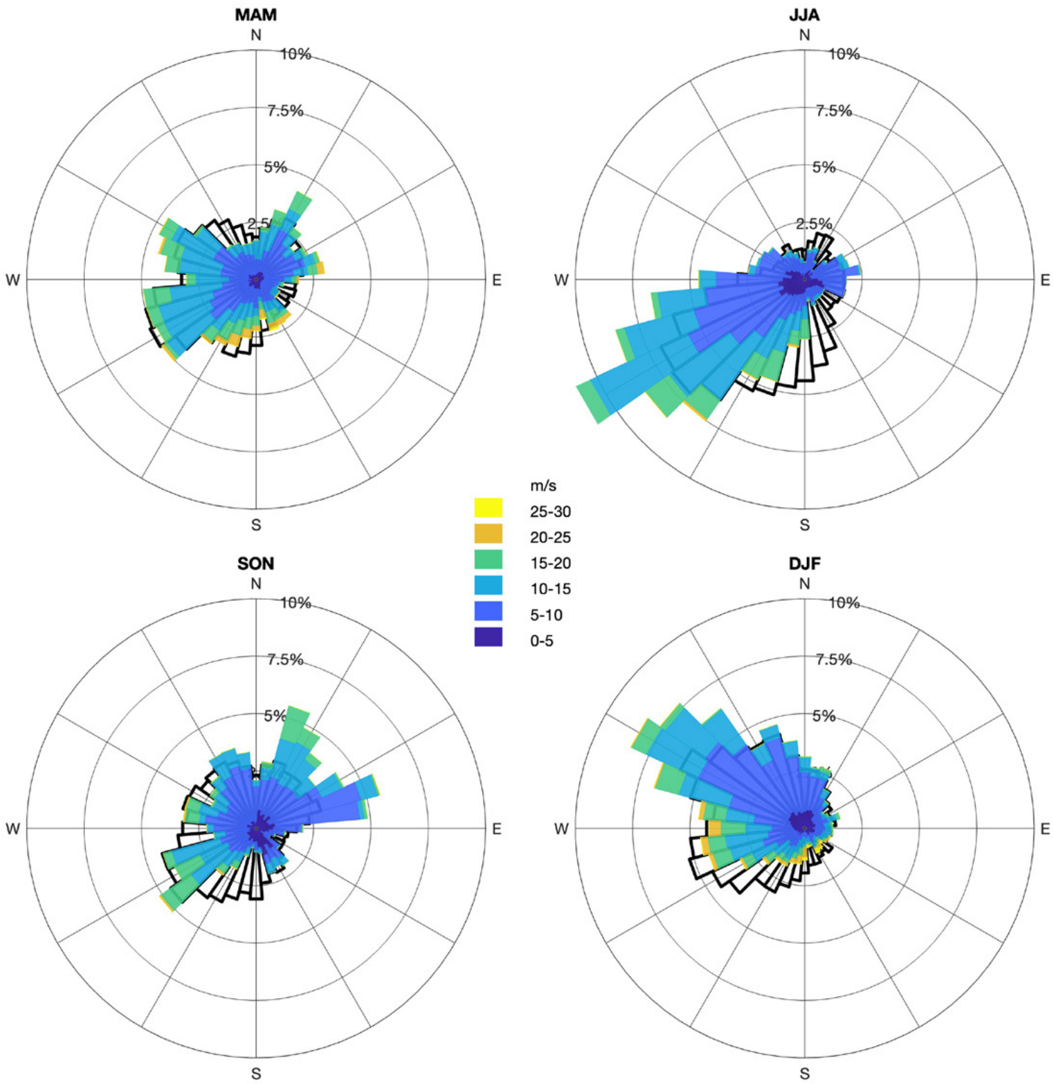

FIG. 2. Seasonal wind speed histograms (shaded colors) at 100 m above sea level from the Air Sea Interaction Tower's (ASIT) vertically profiling Doppler lidar during the study period, November 2023 to August 2025, over the (black outline) climatological seasonal wind speed histograms, based on 9 years of lidar observations at ASIT. Seasons were defined as (MAM) March–May, (JJA) June–August, (SON) September–November, and (DJF) December–February. Data from Cinquino and Kirincich (2024).

horizontal density gradients, guide and distribute ocean surface currents on scales of tens of kilometers or less (Fig. 3), making a heterogeneous boundary condition to the atmosphere above.

Accepted for publication in *Bulletin of the American Meteorological Society*. DOI 10.1175/BAMS-D-25-0201.1.

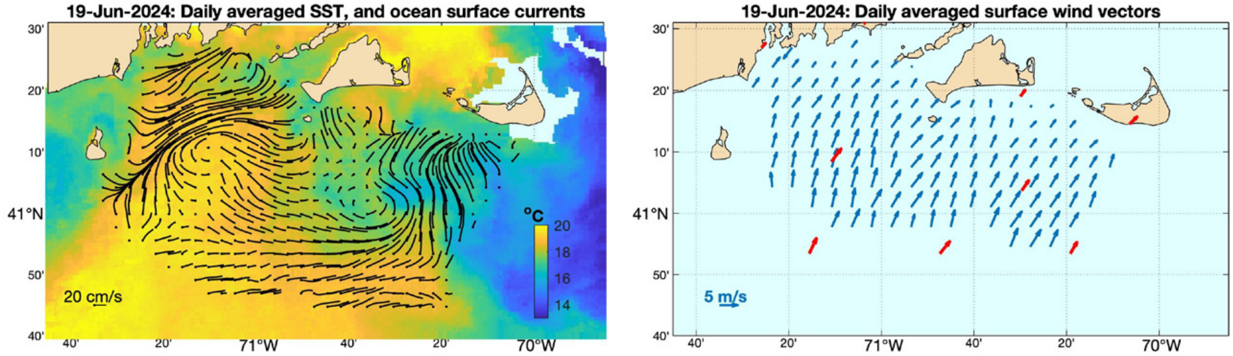

Fig. 3. (left) Daily averaged SST (from NOAA Coastwatch) and ocean surface current streaklines from the Woods Hole Oceanographic Institution's High Frequency Radar (HFR) Array (Kirincich et al. 2022). (right) Atmospheric surface winds for the same day from (red) land or buoy sites and (blue) the HFR array following (Kirincich and Emery 2026). In both panels, only every other HFR grid point is shown for clarity.

The MABL in the region is influenced by a range of phenomena, including mesoscale flows of air masses leaving the continent, storms and squalls (Lombardo and Colle 2012, 2013), sea-breeze circulation with varying roughness and boundary layer structure (Lombardo et al. 2016; Xia et al. 2021), varying ocean surface temperatures (Lentz et al. 2003; Wilkin 2006; Farrar et al. 2007), and wave-modulated air-sea exchange (Sullivan et al. 2008; Edson et al. 2013; Zippel et al. 2024). Winter storms can experience rapid intensification as cool, dry air is advected over a warmer ocean (Skyllingstad and Edson 2009), while spring and summer advection of warm, moist air over a cooler ocean leads to persistent stable boundary layers, LLJs (Mahrt et al. 2014; Jiang and Edson 2020), and fog (Edson et al. 2007). SST gradients in the region can be as large as 6°C over 5 km (Hong et al. 2009), potentially leading to large heterogeneity in the structure of MABL stability.

Thus, the study area demonstrates several of the complexities that are key to advancing our understanding of the marine atmosphere and our ability to resolve it within numerical models. Given the strong changes in ocean surface temperatures across the Northeast Shelf and the resulting heterogeneous atmospheric stability, ocean-level fog and low-level clouds are a persistent feature that can be challenging to forecast correctly. The scales of LLJs, internal boundary layers, and smaller-scale sea-breeze structures are poorly resolved within models of the coastal zone. Finally, the impact of precipitation events on the coupled boundary layer and heat flux between the ocean and atmosphere can be missed by coarse parameterizations. These shortcomings in model physics

Accepted for publication in *Bulletin of the American Meteorological Society.* DOI 10.1175/BAMS-D-25-0201.1.

arise from the lack of observations directly measuring the exchange of momentum, heat, and mass across the coupled boundary layers at adequate spatial and temporal resolution (Shaw et al. 2022).

3. Field Components

The WFIP3 field study had two goals: (1) conduct detailed sampling of the vertical structure of the MABL in order to evaluate and refine model parameterization schemes and (2) carry out wide-area sampling of the MABL to resolve key regional processes and inform and guide model validations. Towards these goals, a multi-platform observational array was deployed to measure:

- Regional atmospheric and oceanographic processes via two lidar buoys, an array of surface flux buoys, and coastal, land-based profiling and scanning observational systems.
- Momentum and heat fluxes at multiple levels above the ocean's surface at two offshore process study sites,
- MABL vertical structure, including velocity, temperature, humidity, and cloud characteristics from remote sensors and rawinsonde launches at fixed coastal sites, offshore anchored platforms, and ship-based transects.

a. Regional Sampling

Coastal Stations: At six shore-based field sites, vertically profiling Doppler lidars, scanning Doppler lidars, thermodynamic profilers, wind profiling radars, surface radiometers (longwave and shortwave radiation), cloud and precipitation sensors, and surface meteorological observations (Table 2, Fig. 4) were deployed by a wide range of project partners. Station locations were chosen to be as close to the coast as possible and to represent the scope of the northern Mid-Atlantic Bight. Sites on the islands of Nantucket (NANT) and Martha's Vineyard (MVCO1&2) as well as at Narragansett, RI, were preexisting Woods Hole Oceanographic Institution (WHOI) coastal radar sites or part of WHOI's Martha's Vineyard Coastal Observatory. The Block Island (BLOC) site was developed by NOAA in partnership with the local airfield, and Truro (CACO) by PNNL as it was used previously during the Two-Column Aerosol Project project (TCAP: Berg 2016). At each station, two scanning Doppler lidars were operated with a coordinated sampling strategy that held one system fixed at vertical stares sampling vertical wind speeds at high temporal resolution

Accepted for publication in *Bulletin of the American Meteorological Society.* DOI 10.1175/BAMS-D-25-0201.1.

Table 2. WFIP3 Station Locations and Equipment

Land-based Stations						
Station	NANT	MVCO1	MVCO2	BLOC	RHOD	CACO
Location	Nantucket	Martha's Vineyard South Beach	Shore Lab	Block Island	Narragansett	Nausett
Latitude (°N)	41.242	41.350	41.360	41.168	41.445	42.03
Longitude (°E)	-70.125	-70.527	-70.525	-71.580	-71.436	-70.049
Coverage Dates	11/2023-8/2025	11/2023-1/2024	11/2023-8/2025	11/2023-8/2025	11/2023-8/2025	11/2023-8/2025
Instruments	Profiling/Scanning Lidars, Thermodynamic Profilers, Wind Profiling Radars, Surface Radiation and Weather					

Surface Buoys					
Station	Sentinel 1	Sentinel 2	Sentinel 3	Sentinel 4	Sentinel 5
Location	Central/ Barge site	Eastern Flank	Offshore/ Outer shelf	Western Flank	Rhode Island Sound
Latitude (°N)	40.892	40.899	40.610	40.900	41.150
Longitude (°E)	-70.800	-70.321	-70.783	-71.267	-71.184
Water depths (m)	52	38	54	61	52
Coverage Dates	2/2024-4/2025	6/2024-4/2025	7/2024-5/2025	3/2024-4/2025	2/2024-8/2024 1/2025-5/2025
Instruments	Air-Sea Fluxes, Surface Meteorology, Surface Hydrography, Waves, Currents*				

	Process Study Sites		Lidar Buoys	
Station	ASIT	Barge or NOAA Ship Pisces	WHOI	DOE/PNNL
Location	2 NM offshore	25 NM offshore	SW corner	NE Corner
Latitude (°N)	41.325	40.900	41.175	40.700
Longitude (°E)	-70.567	-70.783	-70.333	-71.133
Water depths (m)	17	52	32	68
Coverage Dates	11/2023-8/2025	6/2024-10/2024 12/2024**	11/2023-8/2025	11/2023-8/2025
Instruments	Air-Sea Flux Profiles Profiling Lidar Ocean Hydrography Meteorology	Air-Sea Fluxes and/or Profiles Profiling/Scanning Lidars Thermodynamic Profilers Cloud and Wind Profiling Radars Meteorology	Profiling Lidar Meteorology	Profiling Lidar Meteorology

*at Sentinel 1,5 only, **NOAA Ship Pisces

– enabling estimates of turbulence (e.g., Berg et al. 2017) – while a second used velocity azimuth display scanning to sample horizontal wind speeds up to 5 km above sea level (ASL). Additional units served as backup for the first two and were used to conduct process study experiments on LLJs and surface layer turbulent structures over the ocean. Thermodynamic profiles from the surface up to 3 km ASL were retrieved using the physical-iterative TROPoe algorithm (Turner and Löhnert 2021) from ground-based infrared spectrometers (Michaud-Belleau et al. 2025) and

Accepted for publication in *Bulletin of the American Meteorological Society.* DOI 10.1175/BAMS-D-25-0201.1.

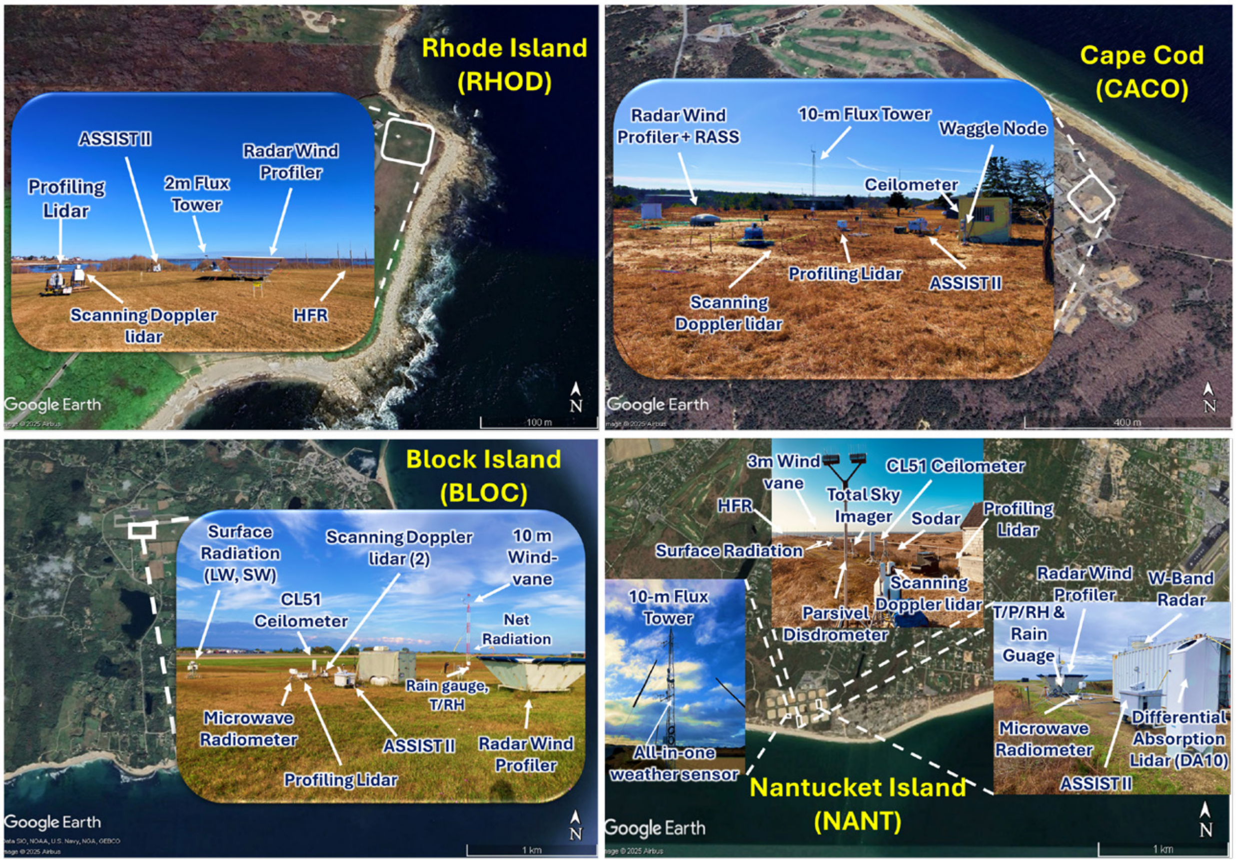

Fig. 4. WFIP3 coastal land observational sites at (clockwise from lower left): Block Island, RI; Nantucket, MA; the Cape Cod National Seashore at Truro MA; and the Rhode Island National Guard Camp Varnum installation in Narragansett, RI. At each site, all deployed instrumentation are shown. Not pictured are installations at the Martha's Vineyard Coastal Observatory (MVCO) on Martha's Vineyard, MA, and the WHOI dock in Woods Hole, MA.

microwave radiometers (Solheim et al. 1998) that were stationed at each location. Ceilometers and W-band radars provided cloud boundaries, while in situ wind sensors, rain and humidity gauges, radiometers, and total-sky imagers provided surface-based wind and meteorological observations.

At-Sea Deployments: Southward and offshore of the coastal land sites, surface buoys were deployed at seven separate locations to collect observations of the coupled atmosphere and ocean. At five locations, 1.5-m-diameter surface "sentinel" buoys were deployed – most frequently by WHOI's R/V Tioga – to measure surface meteorology, turbulent fluxes, wave spectra, and ocean temperature and salinity. The sentinel buoys were distributed across the horizontal array to resolve

Accepted for publication in *Bulletin of the American Meteorological Society*. DOI 10.1175/BAMS-D-25-0201.1.

the multiscale variations in atmospheric and oceanic conditions at the air-sea interface and air-sea exchanges present. As designed, the buoys made measurements 2 m above the surface from multiple redundant anemometers, all with minimal flow distortion (Schlundt et al. 2020; Bigorre et al. 2013), as well as surface air temperature, specific humidity, pressure, precipitation, and downwelling solar and infrared radiation. Sentinel buoys were initially deployed at each site and then removed, serviced, and redeployed at least once during the observational period to extend their measurement life (Table 2).

Two buoy-based ZX M300 lidar wind profilers were positioned both upstream and downstream of a central site, the barge and Pisces site (Fig. 1), relative to the predominant wind direction during summer months and sampled horizontal winds at heights up to 250 m ASL. The larger buoys required to support and power the ZX lidars, a 2.8-m buoy (WHOI: Colbo and Weller 2009; Farrar et al. 2015; Schlundt et al. 2020) and a 7-m (DOE: Sheridan et al. 2023) NOMAD buoy (Timpe and Van de Voorde 1995), were deployed from larger vessels, such as the R/V Armstrong, for a single deployment each. The WHOI lidar buoy sampled surface meteorology in addition to the lidar-based winds. Notably, the WHOI lidar was duty-cycled, sampling the first 30 minutes of each hour, to limit the overall power requirements and therefore the size of the buoy. The DOE buoy supported surface meteorology observations, the lidar, bat sensor, cameras, and a real-time flux-covariance sensor package. All sampled continuously throughout the buoy's deployment period (Table 2). While the WHOI buoy lidar was validated against a tower-validated lidar system on land at the WHOI dock prior to deployment, the DOE lidar buoy was deployed at sea next to WHOI's ASIT (described next) and validated within the buoy against WHOI's lidar prior to being moved offshore.

b. Process Study Sites

Long-term sampling of the vertical structure of the near-surface atmosphere over the ocean was carried out at two locations within the study area. First, ongoing observations (including profiling lidar-based winds, Cinquino and Kirincich 2024) collected at the ASIT, a 27-m-tall fixed structure located 3 km south of Martha's Vineyard in 17 m of water, were augmented as part of WFIP3 to capture the vertical structure of momentum fluxes over the ocean. Direct covariance flux estimates were obtained at multiple levels between 7 and 27 m ASL (Fig. 5), along with surface

Accepted for publication in *Bulletin of the American Meteorological Society*. DOI 10.1175/BAMS-D-25-0201.1.

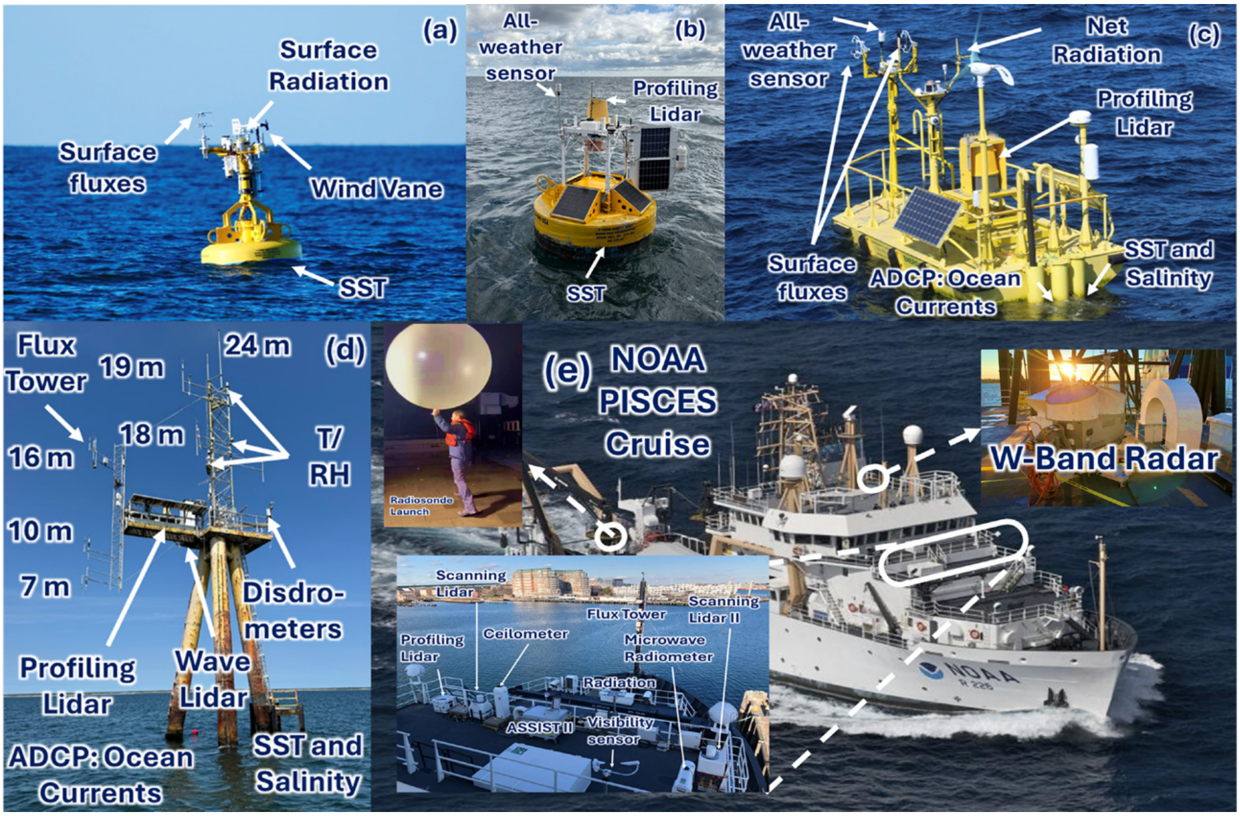

Fig. 5. WFIP3 offshore platforms and buoy systems, including (a) WHOI sentinel surface buoy, (b) WHOI lidar buoy, (c) DOE lidar buoy, (d) WHOI Air-Sea Interaction Tower (ASIT) and (e) NOAA Pisces winter cruise.

meteorology, droplet size distributions, and precipitation rates. Ocean observations collected at the ASIT included surface gravity waves, ocean current profiles, and near-surface and near-bottom ocean temperature and conductivity. Importantly, ASIT observations were made over the full study period, from November 2023 through August 2025.

Secondly, during the spring and summer of 2024, a 46-m barge (Fig. 6) was moored at the central offshore site to collect a full suite of MABL observations from a stable, low-flow distortion platform. The barge was mobilized in April and May of 2024, deployed 25 nautical miles (NM) offshore at a water depth of 52 m in June, and recovered for the last time in late September, completing 85 days of unattended sampling on-station. Two mid-season recoveries and redeployments took place due to forecasted sea state conditions that exceeded the barge's rated sea state limit of 4.5 m (15 ft) for significant wave height.

Accepted for publication in *Bulletin of the American Meteorological Society*. DOI 10.1175/BAMS-D-25-0201.1.

Mobilizing and deploying the barge were significant components of the overarching project. The heavy mooring system specially designed for the WFIP3 barge spanned 1 NM^2 in area and required dedicated winches and handling equipment on the barge and multiple vessels to deploy, maintain, and recover. A hybrid solar-battery-diesel power system was installed to power the 7-kW total sensor load continuously for the entirety of the mobilization period. The power system utilized 30 kW of solar panels mounted on raised supports above the barge deck (Fig. 6); an integrated 100-kWh uninterruptible power supply and battery system composed of five separate 20-kW battery/inverters connected in parallel with a common controller; and two linked 40-kW industrial diesel generators for backup charging and emergency power. These components were integrated onto the barge by WHOI, who ran the barge deployment, power, and satellite communications system.

Moored facing south, the barge's 25-m observational tower allowed low flow distortion observations of the predominant southwesterly winds present from five measurement heights, with observations that matched the ASIT, including momentum, heat, mass, and radiative fluxes. On two raised instrument platforms, remotely sensed observations of wind and thermodynamic profiles through the boundary layer were collected by a series of profiling and scanning Doppler lidars, an infrared spectrometer, a ceilometer, and a W-band radar (Table 2). In addition, the barge supported a micro rain radar for droplet size distribution and precipitation rate profiles, surface meteorological sensors, and thermal imaging cameras and radars for bird and bat detection. While the motion of the barge was dramatically reduced from that of a buoy or ship due to its mooring system, multiple inertial motion units were used to compensate instruments for those motions that existed.

c. Ship Transects and Soundings

Throughout the 18-month field campaign, six intensive operating periods were organized around opportunistic vessel transects through the study area and project-specific offshore sampling via the barge or the NOAA Ship Pisces deployments to the same central site. Within each period (Table 3), radiosondes were launched from a land site in Woods Hole, MA, and from vessels offshore during three of the six periods. During the spring and fall of 2024, a ship transecting the study area from north to south (Fig. 1) launched atmospheric soundings at the same time as the land-based soundings and collected observations on the cloud and wind conditions via ceilometers and scanning and profiling Doppler lidars. During the winter 2024 period, coordinated soundings

Accepted for publication in *Bulletin of the American Meteorological Society.* DOI 10.1175/BAMS-D-25-0201.1.

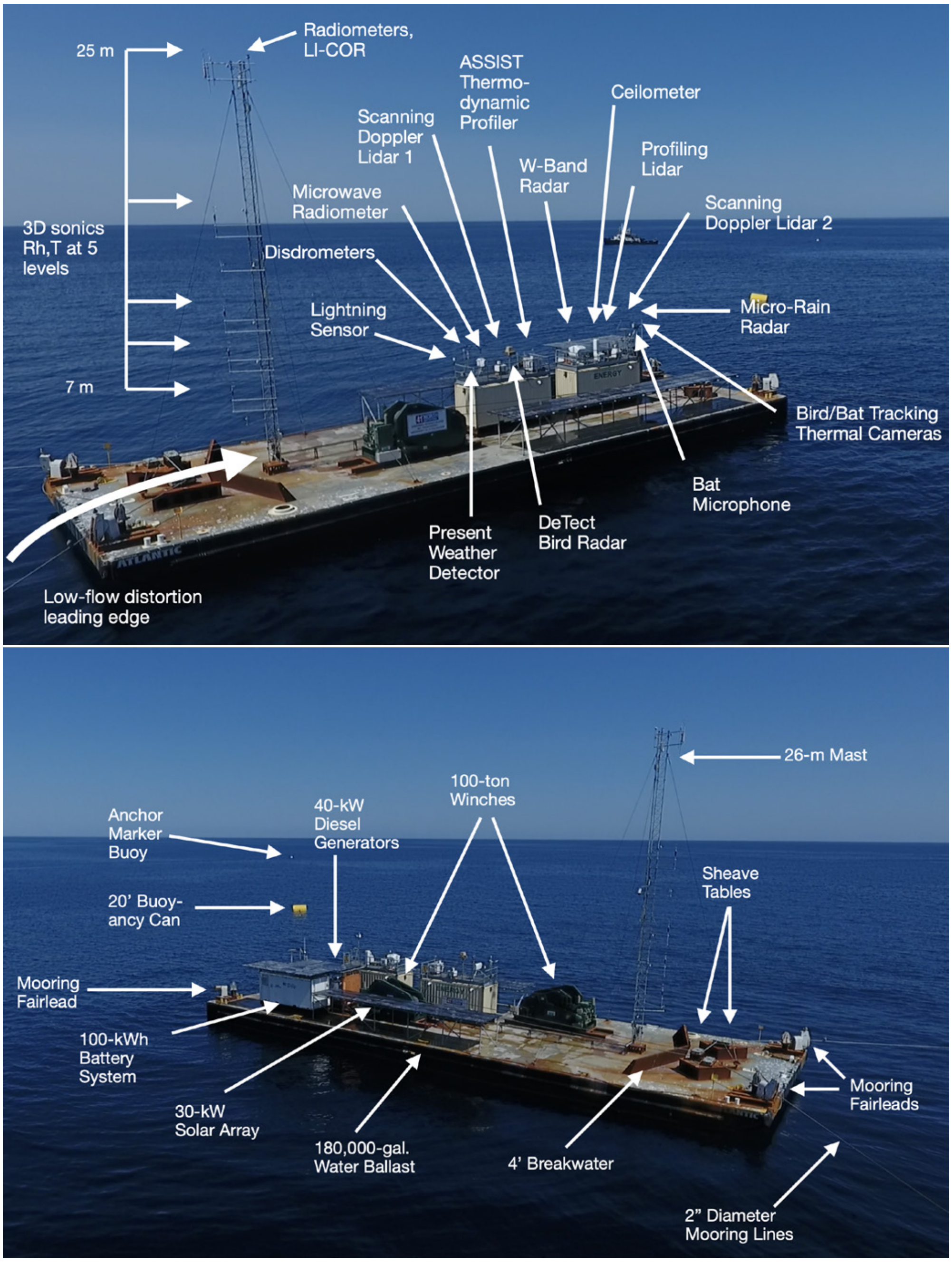

FIG. 6. WFIP3 barge as deployed, showing (top) the mooring system and power components and (bottom) the sensor deployment locations and conditions. The barge platform was anchored 25 NM south of Martha's Vineyard during the summer of 2024.

were conducted from WHOI and from the NOAA Ship Pisces, stationed at the location of the

Accepted for publication in *Bulletin of the American Meteorological Society*. DOI 10.1175/BAMS-D-25-0201.1.

Table 3. WFIP3 Intensive Operating Period Soundings

Intensive Period	Dates	Nominal Launch Times	Total Soundings	Ship
Spring Transect	4–6 May 2024	00/06/12/18Z	24	*R/V Endeavor*
Summer Barge	15–29 July 2024	00/12Z	30	
Fall Barge	21 Sept.–4 Oct. 2024	00/12Z	28	
Fall Transect	7–11 Nov. 2024	00/06/12/18Z	24	*R/V Atlantic Explorer*
Winter Station	5–18 Dec. 2024	00/12Z	28	*NOAA Ship Pisces*
Spring Launches	10–24 Mar. 2025	00/12Z	30	

barge for ~14 days. Observations were also made for aerosols and clouds, surface meteorology and fluxes, scanning and profiling Doppler lidar-based winds, and thermodynamic MABL profiles.

4. Data Products and Data Availability

a. Event Log

Throughout the field period, the WFIP3 project team identified and cataloged events of significance for atmospheric research and forecast assessments, including land-sea breeze events, LLJs, lulls, fog and precipitation, and significant forecast misses. This activity was patterned after a similar effort associated with WFIP2 (Shaw et al. 2019). Weekly analysis of the observed atmospheric state and the quality of the existing NOAA High-Resolution Rapid Refresh (HRRR; Dowell et al. 2022) forecast for the period was undertaken by a rotating member of the WFIP3 team with additional support from the local NOAA weather forecasting offices at Upton and Boston. Team members ranked each day according to the uniqueness of atmospheric conditions and forecast skill. The full quantitative criteria – including specific thresholds used for lidar-based automated detection of low-level jets, weak wind conditions, extreme wind veer, and wind ramp events – can be found in (Bodini et al. 2026). The collective summary of these weekly weather analyses was formulated into an "event log" of weather and ocean events (available at Bodini et al. 2024) that serves as a record of important events for the field campaign and potential case studies for further analysis via observational or modeling studies. As detailed in (Bodini et al. 2026), significant events with poor forecast skill were more prevalent during the warmer months spanning April to September. This is consistent with the dominance during this period of thermally-driven phenomena such as LLJs, sea breezes, and stability-mediated boundary-layer transitions that are known to challenge

Accepted for publication in *Bulletin of the American Meteorological Society.* DOI 10.1175/BAMS-D-25-0201.1.

operational NWP models in coastal environments. These processes depend critically on accurate representation of marine surface fluxes and boundary-layer stability, areas where models such as the HRRR exhibit documented deficiencies over coastal waters (Olson et al. 2019a). Thus, the high-resolution observations collected by WFIP3 during these periods represent particularly valuable targets for model evaluation and improvement, and ongoing analyses are examining specific cases of forecast under-performance identified through the event log.

b. Unified Wind and Thermodynamic Profiles

Unified wind and thermodynamic profiles were developed for each observational site by combining data from multiple sensors into a single estimate of the atmosphere's state, extending from the surface to the top of the boundary layer. Composite wind and atmospheric turbulence profiles relied on a multi-instrument suite of fixed and profiling systems, including scanning and profiling lidars, 915-MHz wind profiling radars, and high-frequency sonic anemometers at each land site. All measurements from each sensor were subject to rigorous quality control procedures such as signal-to-noise ratio filtering, tilt and compass error corrections, thresholding of the ensemble averages for minimum data returns, etc. Two separate data products were generated for potential users: The first, WINDPROF (following Newsom and Krishnamurthy 2022; Krishnamurthy et al. 2013), provides standardized 10-min resolution data, linearly interpolated to a uniform height grid with vertical spacing of 20 m near the surface and 30 m above 100 m above ground level (AGL), for horizontal wind speed, horizontal wind direction, vertical velocity, turbulence intensity, and variances of U, V, and W, each with uncertainty estimates following Newsom et al. (2017). The second, WINDoe (following Gebauer and Bell 2024), uses variational retrieval techniques to provide 30-min averaged horizontal wind speed, horizontal wind direction, and relevant uncertainty estimates (Gebauer and Bell 2024) every 15 minutes on a uniform 10-m-height grid. Using these unified products, atmospheric wind profiles can be examined across a range of temporal and spatial scales, with a comparison of seasonal median profiles at Block Island and Nantucket illustrating the seasonality of upper level winds during the field campaign (Fig. 7).

For unified thermodynamic profiles across each observational site, the TROPoe algorithm (Turner and Löhnert 2014; Turner and Blumberg 2019; Turner and Löhnert 2021) was applied across all thermodynamic profiler and surface meteorological observations collected during the field

Accepted for publication in *Bulletin of the American Meteorological Society.* DOI 10.1175/BAMS-D-25-0201.1.

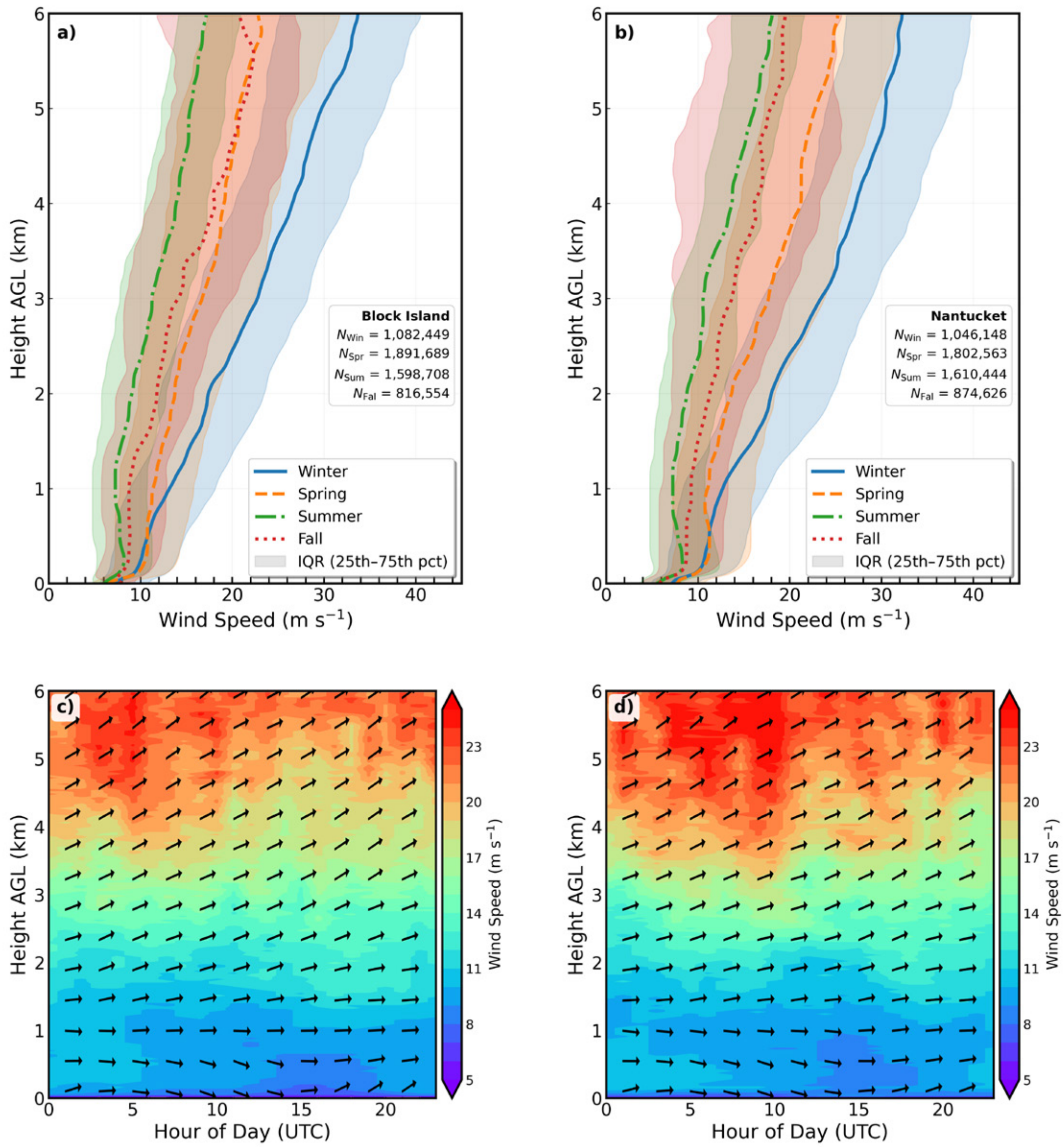

Fig. 7. Seasonally averaged *WINDPROF*-estimated wind profiles at (a) Block Island and (b) Nantucket. Solid lines show the median wind speed for each season (Winter, Spring, Summer, Fall), with shaded regions indicating the interquartile range (IQR; 25th–75th percentile). The number of valid (time, height) observations contributing to each seasonal profile is annotated in the inset boxes. Panels (c) and (d) show diurnal variations in wind speed and direction at Block Island and Nantucket, respectively, aggregated across all available data within the analysis period (February 2024–September 2025). Colored contours show median hourly wind speed; black arrows indicate mean horizontal wind vectors (u, v components).

Accepted for publication in *Bulletin of the American Meteorological Society.* DOI 10.1175/BAMS-D-25-0201.1.

campaign. TROPoe is well established as a reliable method to derive thermodynamic profiles from ground-based remote sensing radiometers, particularly under variable atmospheric conditions (Adler et al. 2023; Blumberg et al. 2017).

c. Buoy Observations

Buoy-based observations of surface winds, surface meteorology, Doppler lidars (on two buoys), and turbulence statistics were compiled from available onboard sensors and relayed in near-real time to shore-based servers as combined observations in 10-min increments. For the DOE lidar buoy, an onboard motion compensation system was developed to compute turbulent fluxes in near-real time (Marcial et al. 2024; Krishnamurthy et al. 2023). Additional post-processing for turbulent fluxes for the other deployed buoy systems is underway.

d. Ocean Surface Currents and Surface Winds

Maps of ocean surface currents were estimated from the observations of a series of four multi-antenna HFRs (Kirincich et al. 2019; Kirincich and Emery 2023) previously deployed in the region at the coastal land sites used for WFIP3 (Fig. 3). Using both radial and elliptical current returns from the fully networked HFRs, the array produces independent, 30-min averages of vector surface currents, having an effective depth of 0.5 m, at 2-km resolution over a 150-km x 80-km area using standard methods (Kim et al. 2007; Clary et al. 2019). RMS differences of the system against the in situ observations were calculated to be ~7 cm s^{-1}. High-resolution estimates of the surface wind field over the study area were also made from the HFR observations following the recent methods of Kirincich and Emery (2026). Independent from the estimated surface currents from the HFR, but at similar range and resolution, the coupled observations of winds and currents at the ocean's surface provide a potentially powerful tool for understanding the coupled system (Fig. 3).

e. Project Data Availability

Data from all sensors, as well as the data products described above, are available for public use via a centralized project-specific download site maintained by DOE (Krishnamurthy et al. 2025). Use of all datasets is highly encouraged, and metadata on individual sensors and products are available via the project database.

Accepted for publication in *Bulletin of the American Meteorological Society.* DOI 10.1175/BAMS-D-25-0201.1.

5. Preliminary Results

Observed atmospheric and oceanic conditions within the study area were representative of the types of conditions and processes present along the U.S. Eastern Coastal Zone (Figs. 2 and 3); thus, the WFIP3 dataset has the potential to address each of the project's objectives. With the field efforts recently completed, preliminary results that address each of the three focus areas described in Section 2a are highlighted below.

a. Surface Wave Processes and Air-Sea Exchanges

Several mechanisms have been suggested to explain the formation of pressure patterns above waves that can lead to wave-coherent momentum fluxes into the atmosphere, including shear instability (Miles 1957; Janssen 1991), flow separation caused by wave geometry (Jeffreys 1925), non-separated sheltering (Belcher 1999), and potential combinations of these processes (Buckley et al. 2025). Earlier field measurements over small, fetch-limited waves strongly supported the shear instability mechanism (Zippel et al. 2024), suggesting that linearly correlated pressure patterns account for the majority of observed pressure variability over waves (Fig. 8a,b) and that shear instability dominates surface pressure variability.

However, observations from the ASIT during WFIP3 offer a striking contrast to these previous results. The long-duration measurements captured numerous occurrences of large intermittent drops in pressure that were measured 90 degrees out of phase with surface waves. In an example of these conditions from a high wave period in December 2023 (Fig. 8c,d), sharp drops in pressure in the lee of wave crests were observed (Fig. 8c: red arrows) that strongly suggest flow separation. These pressure patterns are direct evidence of form drag on the surface, which rapidly transitions into turbulent momentum flux above the surface (Chang et al. 2025). The form drag is therefore critical in governing the total fluxes of momentum, heat, and moisture across the air-sea interface (Bidlot and Janssen 2024). Additional efforts are investigating the interactions between high winds, wave geometry, and turbulent exchanges at the interface to better understand the complex interplay of wind and wave dynamics, form drag, and fluxes during high-energy conditions.

Accepted for publication in *Bulletin of the American Meteorological Society.* DOI 10.1175/BAMS-D-25-0201.1.

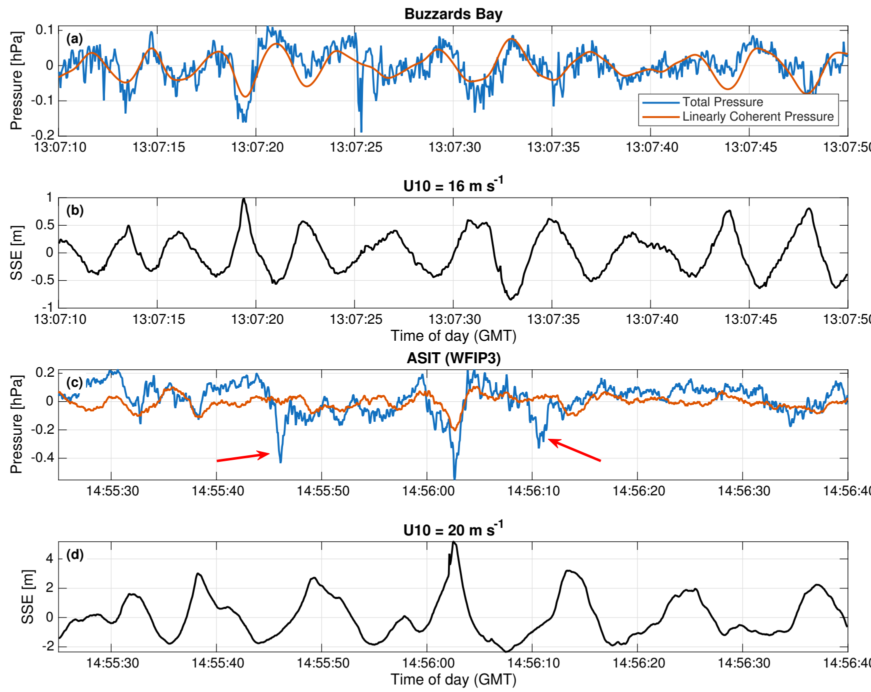

Fig. 8. (a,b) Example of (a) pressure variability and (b) sea surface elevation over small, fetch-limited waves, along with the component of the pressure that is explained with a linear Fourier filter between pressure and wave elevation (orange line in a), highlighting the significant role of shear instability in setting pressure patterns (from Zippel et al. 2024). (c,d) Comparative example of large-wave pressure and sea surface elevation collected at ASIT during WFIP3. Here, numerous pressure drops were observed that were 90 degrees out of phase with surface waves (red arrows) and not explained with a linear Fourier filter, suggesting the prevalence of intermittent flow separation, and form drag processes during extreme wind events.

b. Summertime LLJs Leading to Marine Fog Events

LLJ formation and maintenance is strongly influenced by land-sea thermal gradients (McCabe and Freedman 2023; De Jong et al. 2024). Frictional decoupling within the atmospheric boundary layer over cold water further enhances wind speeds at lower altitudes, often leading to very shallow LLJs (Debnath et al. 2021; Quint et al. 2025) in coastal regions. However, the interplay of LLJ formation and the occurrence of marine fog, a critical weather phenomenon for operational use of the coastal zone, is understudied.

Within the WFIP3 campaign, numerous LLJ conditions were observed and marked as critical forecast events (Bodini et al. 2026), many of which also exhibited fog formation. As an example, the

Accepted for publication in *Bulletin of the American Meteorological Society*. DOI 10.1175/BAMS-D-25-0201.1.

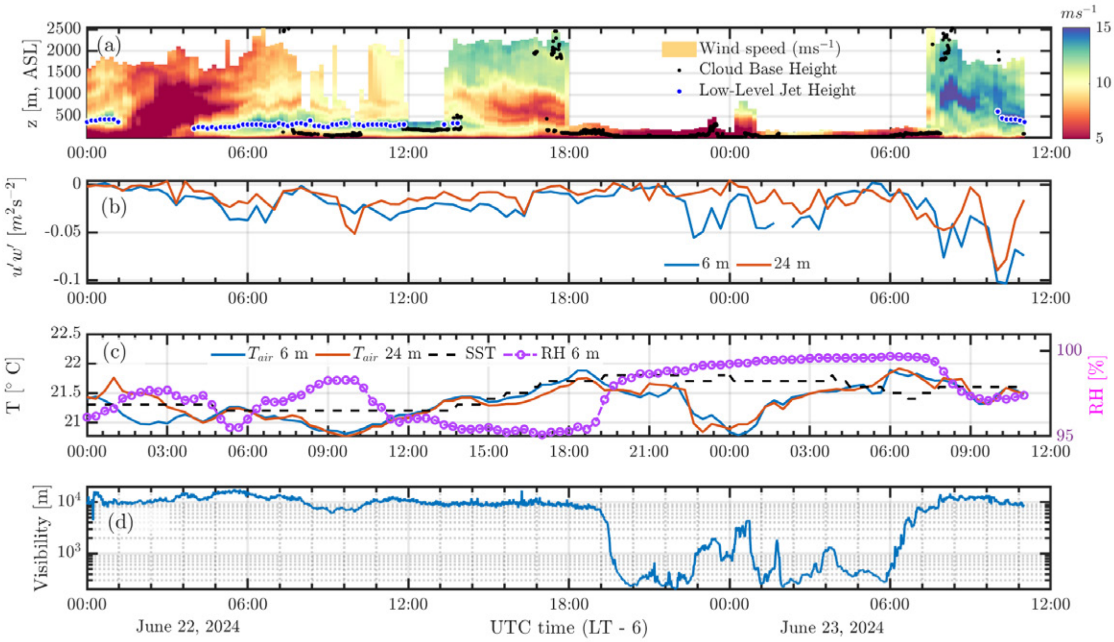

Fig. 9. Barge-based observations of (a) merged horizontal wind speed profiles from Doppler lidars and cloud base height from Ceilometer, (b) vertical momentum flux, (c) air temperature and relative humidity (RH) from 6 and 24 m above sea level (ASL) from the barge tower along with SST from the nearby Sentinel 1 buoy, and (d) near-surface visibility measured at the barge, all from 22–23 June 2024.

LLJ event observed on 22–23 June 2024 was coupled with the downward advection of temperature and moisture, leading to sustained marine fog near the barge location. This jet appeared ~250 m ASL (Fig. 9a), beginning at 0500 UTC (0000 EST) on 22 June and persisted for 7 hours. Overnight, radiative cooling of nearby land surfaces likely increased the stability of the MABL, effectively trapping moisture near the surface. The advection of moisture-rich air along the LLJ path and warm air advection from the coast enhanced relative humidity at the surface across both the marine environment and adjacent coastal areas. The onset of sunrise on 22 June initiated radiative heating (Fig. 9c), which progressively weakened boundary layer stability. This destabilization led to vertical mixing of the atmospheric layers, redistributing the trapped moisture closer to the surface. As temperatures reduced sufficiently and the air reached saturation, condensation occurred, resulting in the formation of fog, noted by the change in visibility at the barge (Fig. 9d).

Accepted for publication in *Bulletin of the American Meteorological Society*. DOI 10.1175/BAMS-D-25-0201.1.

Additionally, the onset and evolution of LLJ events during WFIP3 was captured via a novel real-time, dynamic sampling framework. The field system, referred to as WaggleDop, autonomously altered the lidar's scan strategy to focus observations on the LLJ heights. The WaggleDop system uses the Waggle Node (Beckman et al. 2016; Jackson et al. 2023), a software-defined edge computer that can directly communicate with connected instruments and upload processed data to a cloud infrastructure. Using the cloud infrastructure, software is deployed to the Waggle Node that sends a user-prescribed scan strategy to the lidar. These scan strategies are based on wind speed and direction criteria, using data from any connected lidar's vertical wind profiles, which are also processed using software deployed to the node. Deployed at NANT and BLOC, the systems were tested during a series of targeted events in June and July 2025 and realized 20 cases using adaptive targeting of LLJs during the study period.

c. Impact of LLJ on Vertical Structure of MABL

Observations from scanning Doppler lidars performing vertical staring measurements and six-beam Doppler beam swinging profiles allow estimation of the turbulence kinetic energy (TKE) dissipation rate ϵ (following O'Connor et al. 2010) and thus a characterization of the vertical variability of ϵ during LLJ conditions at longer ranges than previously done by Bodini et al. (2019a). For onshore unstable conditions, the vertical variability of ϵ typically presents a roughly monotonic reduction with increasing height associated with the wind speed increase and the reduction of turbulence intensity due to the reduced wind shear. In contrast, during the occurrence of an LLJ, these components are competing (Bodini et al. 2019b), thus leaving the vertical variation of ϵ rather unpredictable. Here, wind speed does not have a monotonic trend with height but a peak observed at the LLJ nose. Additionally, the increased shear in the proximity of an LLJ's nose can lead to an increase in mechanically produced turbulence. On the other hand, the stable atmospheric conditions associated with the generation of LLJs generally lead to a disruption of turbulence and a reduction in the turbulent fluctuations of the wind vertical velocity. As a result, TKE dissipation rate can either increase or decrease during the occurrence of an LLJ depending on the balance among these various physical contributions.

In Fig. 10, we contrast the vertical variability of wind speed, TKE dissipation rate, and air temperature observed during an event characterized by an unstable atmospheric regime (Fig. 10:

Accepted for publication in *Bulletin of the American Meteorological Society.* DOI 10.1175/BAMS-D-25-0201.1.

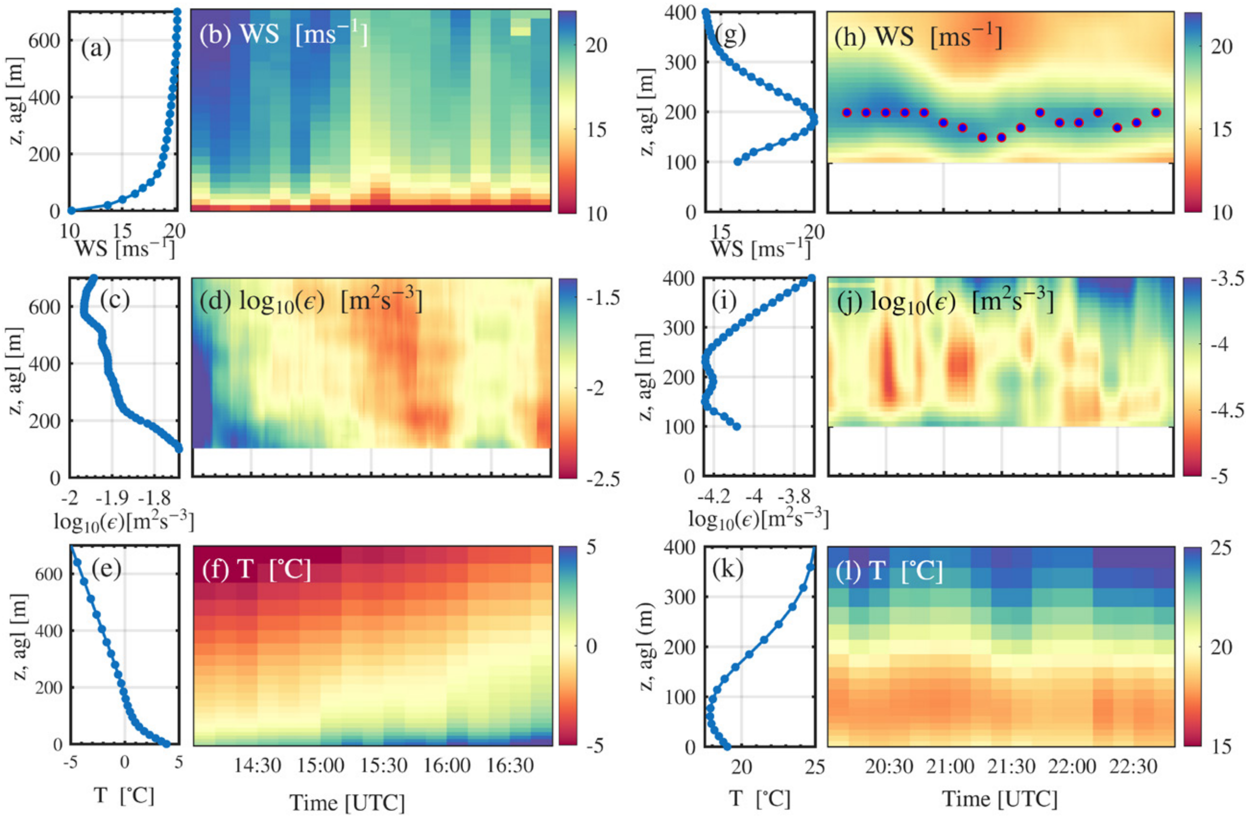

FIG. 10. Profiles above ground level (AGL) of (top) wind speed, (middle) ϵ, and (bottom) temperature collected at Nantucket on (left) March 7, 2025 under unstable atmospheric regime and (right) June 22, 2025 under the occurrence of an LLJ. For each panel the mean vertical structure is shown at left with a 3-hour timeseries from the day at right.

left) with a stable case in which an LLJ was present (Fig. 10: right). For the unstable case, a roughly monotonic variation of the considered physical parameters is observed, namely, a gradual increase with height of wind speed (Fig. 10a,b), associated with a reduction in ϵ (Fig. 10c,d), and air temperature (Fig. 10e,f). For the stable case, the LLJ nose is observed at a height of about 180 m (Fig. 10g,h), which corresponds to a region with a minimum TKE dissipation rate (Fig. 10i,j), while the air temperature achieves a minimum below the LLJ nose (~85 m) and increases aloft (Fig. 10k,l). This analysis suggests that the increase in streamwise momentum (Fig. 10g,h) and a reduction of turbulent activity in the proximity of the LLJ nose leads to a reduction in ϵ (Fig. 10i,j). Therefore, the increased shear associated with an LLJ and the associated mechanically produced turbulence provide a minor contribution to the turbulence characteristics of this LLJ.

Accepted for publication in *Bulletin of the American Meteorological Society*. DOI 10.1175/BAMS-D-25-0201.1.

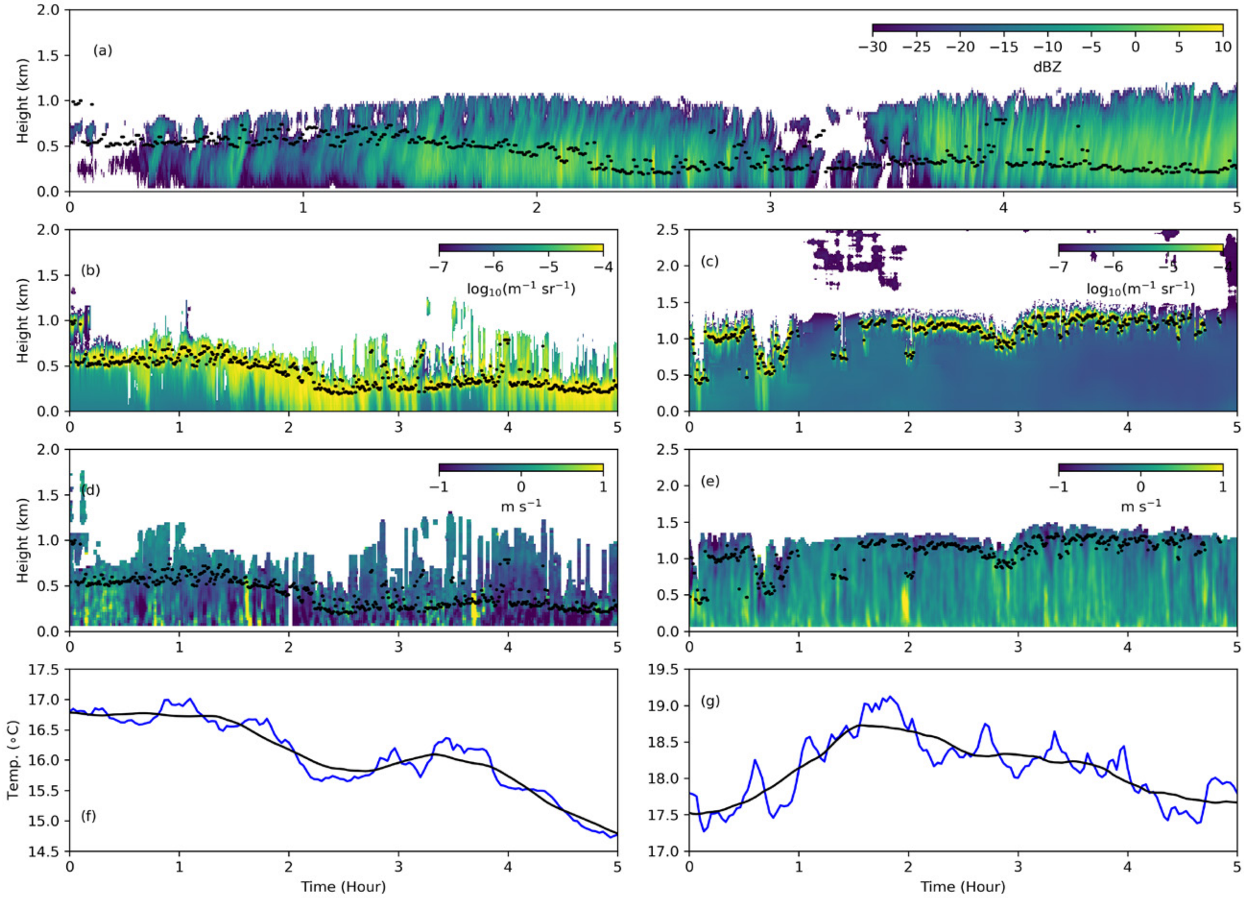

FIG. 11. Time-height profiles of (a) radar reflectivity at Nantucket, lidar backscatter from ceilometers at (b) Nantucket and (c) Block Island, vertical air motion as reported by Doppler lidars at (d) Nantucket and (e) Block Island, and instantaneous (blue) and background (black) 2-m air temperature at (f) Nantucket and (g) Block Island, all starting at 06 UTC on 22 Sept. 2024. Positive velocities in (d) and (e) denote updrafts.

d. Rain-Induced Cold Pools

Precipitation evaporates in sub-saturated layers below cloud base, thereby cooling and moistening the sub-cloud layer and hence stabilizing it. The evaporative cooling is associated with modifications to turbulence, the potential strengthening of downdrafts, and the formation of cold pools or density currents (Zuidema et al. 2017). Rain-induced cold pools are known to impact cloud and precipitation mesoscale structure making them important for accurately forecasting precipitation, turbulence intensity, and surface meteorology (Benjamin et al. 2018).

Observations during a 5-hour period from 22 September 2024 starting at 06 UTC (midnight local time) are used to showcase rain-turbulence-cold pool interactions during WFIP3 (Fig. 11). Post-

Accepted for publication in *Bulletin of the American Meteorological Society*. DOI 10.1175/BAMS-D-25-0201.1.

cold-frontal stratocumulus clouds were observed over the land sites during this period, and deep stratiform rain was present at the barge location. The vertically pointing cloud radar at Nantucket reported a precipitating stratocumulus cloud with top around 1 km and precipitation reaching the surface and cloud base lowering gradually from 500 m at the beginning of the case to 100 m at the end. The ceilometer present at Nantucket captured the cloud base height and below-cloud precipitation with backscatter values in excess of 10^{-4} m^{-1} sr^{-1}, indicative of drizzle or light rain. The ceilometer at Block Island reported a low-level stratus cloud devoid of any precipitation. The profiling Doppler lidars at both sites reported a turbulent boundary layer with updrafts and downdrafts in excess of ±1 m s^{-1}. However, due to presence of precipitation at Nantucket, the variance of vertical air motion was much higher at Nantucket (0.35 m^2 s^{-2} at 200 m) than at Block Island (0.05 m^2 s^{-2} at 200 m), with strong downdrafts often associated with drizzle shafts. It should be noted that strong updrafts were observed at Nantucket at the leading edge of the drizzle shafts, consistent with previous observations and modeling studies. The 2-m air temperature decreased by ~3 K at Nantucket during this period, while it fluctuated between 17–19°C at Block Island. The instantaneous 2-m air temperature at both locations was affected by the turbulence, with higher-than-background temperatures associated with updrafts and colder-than-background temperatures during downdrafts. As illustrated here, rain-turbulence-surface meteorology interactions were well observed during WFIP3, and the observations can be analyzed to derive quantitative estimates of drizzle-induced evaporative cooling and its impact on cold pool formation.

e. Cold Front Passages

While each of the intensive operating time periods in 2024 had notable events including cold fronts on 2 September, 27 September, 8 November, and 12 December, for example, here we focus on a cold front following a series of strong temperature inversions, LLJs, and low cloud cover that were not well forecasted by the HRRR from 25–29 September 2024. Before the passage of the cold front on 27 September (Fig. 12a,c), atmospheric sounding observations from the WHOI station showed predominantly easterly (onshore) winds below and westerly (offshore) flow above persistent temperature inversions, providing favorable conditions for low clouds (Fig. 12d). The system was accompanied by multiple LLJs between 300 and 550 m, with LLJ cores > 12.5 m s^{-1} on 25 September and 29 September and a core of > 17.5 m s^{-1} on 27 September at 00Z (Fig. 12a).

Accepted for publication in *Bulletin of the American Meteorological Society*. DOI 10.1175/BAMS-D-25-0201.1.

After the passage of the cold front, northerly winds were observed. Then, a stationary front off the mid-Atlantic coast and Hurricane Helene to the south conspired to produce moderate easterly boundary layer flow below westerly flow, similar to the wind conditions observed before the cold front. The thermodynamics revealed a significantly dry air mass at the beginning of the observation period that warmed and moistened with a warm frontal passage and then cooled and dried with a subsequent cold frontal passage (Fig. 12b,c). While each LLJ was associated with inversions, the two LLJs on 29 September at 00Z were the only ones observed with an inversion capping the LLJ, with one at 550 m (3 K increase between 550–600 m) and the other at 1.2 km (2.5 K increase between 1.2–1.4 km) (Fig. 12b). A strong inversion was also seen at 1.5 km in the 28 September 00Z sounding, with a corresponding drop in aerosol signal in ceilometer backscatter (Fig. 12d). Using observations from the event log, the HRRR accurately reproduced the observed shift from easterly to westerly winds prior to the cold frontal passage but underestimated the uptick in wind speeds associated with the LLJ on 27 September and was not able to resolve the strong capping inversion at 1.2–1.4 km observed from 27–29 September.

6. Implications for Modeling and Prediction

The WFIP3 observational campaign was specifically designed to enable detailed modeling studies of the events and conditions present within the study area and to provide validation data for advanced parameterizations, model coupling, and model skill assessments. Modeling efforts underway now seek to improve hindcast and forecast estimates of the MABL, air-sea coupling, and wind events by improving model physics and model coupling via quantitative evaluation of these improvements for key conditions or events using the field study observations. Initial work in these efforts is detailed below.

a. HRRR Comparisons

The High-Resolution Rapid Refresh (HRRR) numerical weather prediction model has been run operationally by the National Weather Service over the U.S. since 2014. The HRRR is based on the WRF-ARW modeling system, and its data assimilation system and physical parameterizations have been continually updated, with version 4 (HRRRv4) being operational since December 2020 (Dowell et al. 2022). It uses a 3-km horizontal grid spacing with 50 vertical levels, and is restarted

Accepted for publication in *Bulletin of the American Meteorological Society.* DOI 10.1175/BAMS-D-25-0201.1.

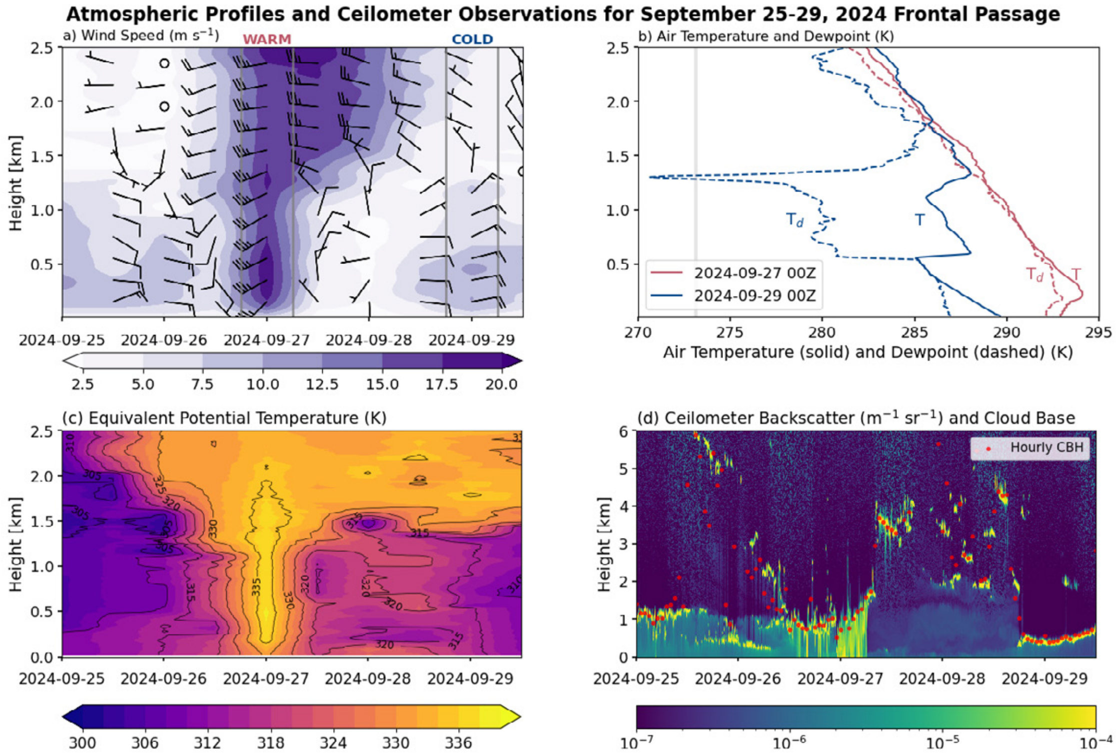

FIG. 12. Atmospheric soundings and ceilometer observations for a cold frontal passage during 25–29 Sept. 2024. (a) Wind speed and wind direction profiles to 2.5 km. Warm and cold markers correspond to profiles in panel b. (b) Temperature and dewpoint profiles before (27 Sept.) and after (29 Sept.) the cold frontal passage. (c) Equivalent potential temperature profiles during the event. (d) Ceilometer backscatter profiles (color) and hourly cloud base height (red dots). To preserve the weak backscatter signal of boundary layer aerosols on 27–29 Sept., no filtering is applied to the data.

hourly (thereby using the latest available observations) providing forecasts out to 18 hr every hour, and forecasts out to 48 hours when the model is initialized at 00, 06, 12, and 18z. The HRRR has been extensively validated with many different datasets (e.g. James et al. 2022), and is considered a foundational model that is used by a range of different stakeholders in their decision making process (e.g. Turner et al. 2022). WFIP3 provides a unique opportunity to extensively evaluate HRRRv4 with observations off the U.S. East Coast, and was one of the primary objectives of this campaign.

Observations from the campaign revealed systematic biases within the HRRRv4 model in predicting wind speed and static stability, with notable seasonal dependencies. Fig. 13 shows differences

Accepted for publication in *Bulletin of the American Meteorological Society.* DOI 10.1175/BAMS-D-25-0201.1.

in wind speed, temperature, and static stability at Nantucket between observations and HRRRv4 from March 2024 through February 2025. At low observed wind speeds, the HRRRv4 tended to slightly overestimate wind speed, transitioning to a negative bias as wind speed increases. The positive bias at low wind speeds has been observed at land-based sites before, and is partially attributed to the fact that wind speed is always non-negative (Fovell and Capps 2024). The bias becomes particularly pronounced for wind speeds greater than 12 m s^{-1}, where deviations exceed 1 m s^{-1}. A portion of the wind speed errors in windy conditions is due to representativeness uncertainties (i.e., mismatches spatially and temporally between point sensors and a 3-km model), or the model's inability to fully capture the temporal variability of the wind field (Fovell and Capps 2024; Fovell and Gallagher 2022). Additionally, underestimation in wind speed is more frequent and larger on average during periods of warmer 2-m temperatures, generally above 13°C. These larger temperature conditions appear to exacerbate the errors, amplifying discrepancies between predicted and observed values. Consistent biases were also observed when comparing solely LLJ events (Bodini et al. 2025; Adler et al. 2026).

Warmer temperatures are also associated with weaker static stability in the HRRRv4 model, resulting in notable negative errors in stability predictions. This relationship suggests a coupling between wind speed and stability errors, wherein larger underestimations in wind speed coincide with more significant underestimations of static stability. These findings highlight seasonal variations in model performance, with stronger biases observed during warmer months. A detailed multi-season evaluation of the HRRR model is presented in Adler et al. (2026). Understanding the interplay between wind speed and stability biases, and how gustiness should vary as a function of stability and wind speed, in the HRRRv4 is critical for improving predictive capabilities, particularly in dynamic atmospheric conditions that dominate warmer seasons.

Extensive modeling studies aimed at model enhancements and reducing biases utilizing the WFIP3 observations have been performed, which will inform forthcoming updates to the HRRR physics suite and its future use in operational forecast products. Specifically, a set of 30 case studies encompassing a variety of event types has been executed iteratively with attempts to modify the model physics, initial conditions, and lower boundary conditions in an effort to diagnose the true source of the simulated biases and demonstrate improvements relative to WFIP3 observations.

Accepted for publication in *Bulletin of the American Meteorological Society.* DOI 10.1175/BAMS-D-25-0201.1.

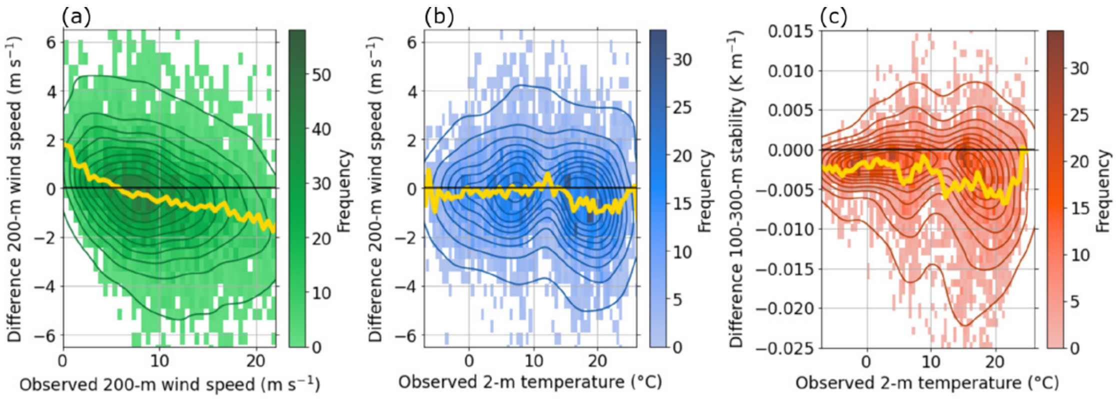

FIG. 13. Difference in wind speed (HRRR model forecast hour 3 minus observation) at 200 m over (a) observed wind speed at 200 m and (b) observed temperature at 2 m. (c) Difference in static stability (HRRR model forecast hour 3 minus observation) over observed temperature at 2 m. Static stability is computed as the virtual potential temperature gradient between 100 and 300 m. The yellow line indicates the bin mean. Data are shown for Nantucket during the period March 2024 through February 2025. Observed temperature and wind profiles are obtained with TROPoe and WINDoe retrievals.

Future publications will detail this model development endeavor, which yield improved low-level wind speed, shear, dynamic stability, and cloud morphology.

b. Importance of Model Coupling

WFIP3 mesoscale modeling efforts established fully coupled regional modeling systems focused on achieving a skillful representation of the coupled ocean–atmosphere–wave climatology characteristic of the region using the Scripps Coupled Ocean–Atmosphere Regional (SCOAR) and Coupled Ocean–Atmosphere–Wave–Sediment Transport (COAWST) modeling frameworks (Seo et al. 2007; Sauvage et al. 2023; Warner et al. 2010; Gaudet et al. 2022), which each implement three-way coupling among WRF, ROMS, and WAVEWATCH III at high resolution. As offshore wind farms entered construction phases, modeling efforts expanded to include wind farm parameterizations within a fully coupled framework, enabling evaluation of wind–wave–SST interactions in the presence of wind energy infrastructure. Sensitivity experiments were conducted to assess suitable ocean–wave–atmosphere coupling formulations as well as the importance of different forcings in an uncoupled model framework, such as SST and meteorological initial conditions (Tai et al. 2025).

Accepted for publication in *Bulletin of the American Meteorological Society.* DOI 10.1175/BAMS-D-25-0201.1.

Initial coupled model simulations show that, under stably stratified conditions, parameterized offshore wind turbine wakes induce small but measurable oceanic responses, including a seasonal-mean SST anomaly of 0.3−0.4°C and a shallower ocean mixed layer depth (Seo et al. 2025). Although small relative to synoptic atmospheric variability and the large seasonal SST cycle in this region (Shearman and Lentz 2010), the upper-ocean temperature response leads to an upward heat flux that destabilizes the model MABL. The resulting enhanced downward momentum transport modestly increases near-surface wind speeds, partially offsetting wake-induced wind speed deficits. Coupled simulations further indicate that wake-driven wind reductions suppress wind wave growth, leading to fetch-dependent changes in significant wave height and wave-supported momentum flux, along with a shift of the sea state toward older wave conditions (Sauvage et al. 2025). Reduced wind–wave growth lowers the effective surface roughness and surface stress, weakening near-surface TKE, shoaling the mixed layer, and reducing entrainment cooling. Ocean mixed layer heat budget analysis identified reduced entrainment cooling as the dominant driver of the wind-wake-induced mixed layer temperature anomaly.

From a model evaluation perspective, fully coupled simulations reduce wind speed and wind direction errors within the lowest 50 m ASL relative to stand-alone WRF configurations and more accurately represent air–sea interaction processes and surface layer dynamics (Huang et al. 2025). These improvements are most pronounced at or near the ocean surface, with diminishing impacts above 50–100 m ASL. As a result, while ocean–wave–atmosphere coupling meaningfully affects near-surface turbulence, its thermodynamic and mechanical feedback influence on time-averaged wind speeds above the surface layer at heights above 100 m, are negligible (Seo et al. 2025; Huang et al. 2025). These results also emphasize the importance of resolving SST and wave roughness to improve coastal wind profiles in the lowest 100 m ASL. Given that NOAA's HRRRv4 model currently uses SST forcings derived from its parent GFS model, which operates at a much coarser resolution, precise SST forcings are paramount for accurately representing atmospheric stability across the domain and for improving surface layer forecasts.

c. Evaluating PBL Schemes

High-resolution gray-zone (horizontal grids 100 m–1 km) modeling will be essential for increasing the accuracy of key coastal and marine atmospheric processes that govern the MABL

Accepted for publication in *Bulletin of the American Meteorological Society.* DOI 10.1175/BAMS-D-25-0201.1.

structure. Preliminary efforts (Jiang 2026) comparing the performance of the 3DTKE (Zhang et al. 2018) and MYNN-EDMF (Olson et al. 2019a, 2026) PBL schemes within the study area were done within a one-way nested WRF model, with maximum horizontal resolution of 300 m and bounded by ERA5, for 17 events in 2024, representing stable, neutral, and unstable boundary layer conditions and cold-air outbreaks. Compared to the ASIT lidar observations (results not shown here), the 3DTKE scheme, developed specifically for gray-zone simulations, performs better than the MYNN-EDMF scheme for all but very stable conditions. 3DTKE also produced systematically lower TKE than MYNN-EDMF and coarser vertical-velocity structures with smaller magnitudes. A 3D PBL scheme (Kosović et al. 2020; Juliano et al. 2022) was evaluated with a focus on cold-air outbreak events. Preliminary results indicate that, when compared to a 1D PBL scheme, simulations with the 3D PBL scheme were able to better resolve convective structures in the gray zone.

7. Conclusions

The third Wind Forecast Improvement Project (WFIP3) has collected a vast amount of observations of the marine atmospheric boundary layer and coastal ocean over the northern component of the Mid-Atlantic Bight. These observations are critical for increasing our understanding of the coupled atmospheric and oceanic system in coastal zones and have implications for improving weather and oceanic forecasting. The long-term goal of the field campaign was to collect observations that enable detailed model development and assessment efforts far into the future. Initial analysis of the results from the project team have illustrated the occurrence of high form drag events at the ocean's surface due to incoherent surface pressures and examined the vertical structure of atmospheric turbulence during both stable and unstable events. Low-level jets and fog events were common during the observational record due to the progression of synoptic-scale weather events, offering a wealth of both challenging and important dynamical conditions to be examined. The project's event log (Bodini et al. 2026) offers a unique summary of weather and other phenomena throughout the study period. These data, data products, and summaries are available for public use and analysis via the open data repository maintained by the Department of Energy (Krishnamurthy et al. 2025). Use of all datasets is encouraged; metadata on individual sensors and products are available via the project database.

Accepted for publication in *Bulletin of the American Meteorological Society.* DOI 10.1175/BAMS-D-25-0201.1.

Efforts to refine and test advanced coupling of atmospheric, wave, and oceanic modeling systems are ongoing beyond the preliminary results described above. A goal of coupled modeling efforts within WFIP3 was to identify the regimes and physical processes with impacts concentrated near the ocean surface that contribute to model improvement in coastal marine environments. Initial results from modeling efforts clarified when full ocean–wave–atmosphere coupling may be required for improved wind forecasts (Seo et al. 2025; Sauvage et al. 2025), and compared PBL schemes. The WFIP3 observations enable further targeted evaluation of these coupled models as well as refinement of wave–atmosphere parameterizations governing surface fluxes and wave–ocean parameterizations controlling upper-ocean turbulence and mixing, supporting physically consistent advances in next-generation coastal prediction systems.

The WFIP3 project team has undertaken and successfully completed a complex, multi-institutional, multi-agency field campaign to observe and understand the critical interactions between the ocean and atmosphere that determine the structure, composition, and dynamics of the marine atmospheric boundary layer. Numerous analysis tasks remain, including wind-wave and wind-wave-ocean model coupling simulations for both case studies and the full period observational that will allow improved representation of winds, waves, clouds, and precipitation in models of the coastal zone. However, the best is yet to come, as future analysis from the broader community will enable scientific advancements based on these datasets for decades to come.

Accepted for publication in *Bulletin of the American Meteorological Society.* DOI 10.1175/BAMS-D-25-0201.1.

Acknowledgments. Funding for the WFIP3 field program was provided by U.S. Department of Energy Office of Critical Minerals and Energy Innovation Wind Energy Technologies Office via cooperative agreements DE-EE0009424 to the Woods Hole Oceanographic Institution, the NOAA ASRE Program via NOAA cooperative agreement NA22OAR4320151 to the Cooperative Institute for Earth System Research and Data Science (CIESRDS), the Massachusetts Clean Energy Center, and internal funds from the Woods Hole Oceanographic Institution. This work was authored in part by the National Laboratory of the Rockies under Contract No. DE-AC36-08GO28308, by the Lawrence Livermore National Laboratory under Contract No. DE-AC52-07NA27344, by Argonne National Laboratory under Contract No. DE-AC02-06CH11357, and by Pacific Northwest National Laboratory (PNNL) under Contract No. DE-AC05-76RLO1830. Ship-based Spring and Fall 2024 intensive period sampling was made possible by NSF support for the Northeast Shelf Long-Term Ecological Research Program (OCE# 2322676). The research team thanks several individuals who supported the field deployments including: E. Cinquino, J. Sisson, I. Fernandez, S. Faluotico, H. Popenoe, A. Scholbrok, D. Jager, J. Wehof, S Miller, M Jacques, J Covert, J Freedman, Ocean Technical Services, and Wind Data Hub team for hosting the observations for this project. The views expressed in the article do not necessarily represent the views of the DOE, NOAA, or the U.S. Government. The U.S. Government retains and the publisher, by accepting the article for publication, acknowledges that the U.S. Government retains a nonexclusive, paid-up, irrevocable, worldwide license to publish or reproduce the published form of this work, or allow others to do so, for U.S. Government purposes.

Data availability statement. Data for all WFIP3 project collected data are available via the centralized repository maintained by PNNL: https://a2e.energy.gov/project/wfip3

References

Adler, A., and Coauthors, 2026: Multi-season evaluation of temperature and wind in the marine boundary layer along the united states northeast coast in the High-Resolution Rapid Refresh model. *Geoscientific Model Development*, **submitted**.

Adler, B., and Coauthors, 2023: Impact of seasonal snow-cover change on the observed and simulated state of the atmospheric boundary layer in a high-altitude mountain valley. *Journal of Geophysical Research: Atmospheres*, **128 (12)**, e2023JD038 497.

Accepted for publication in *Bulletin of the American Meteorological Society.* DOI 10.1175/BAMS-D-25-0201.1.

Aird, J. A., R. J. Barthelmie, T. J. Shepherd, and S. C. Pryor, 2022: Occurrence of low-level jets over the eastern U.S. coastal zone at heights relevant to wind energy. *Energies*, **15**, 445, https://doi.org/10.3390/en15020445.

Archer, C. L., B. A. Colle, D. L. Veron, F. Veron, and M. J. Sienkiewicz, 2016: On the predominance of unstable atmospheric conditions in the marine boundary layer offshore of the U.S. Northeastern coast. *Journal of Geophysical Research: Atmospheres*, **121 (15)**, 8869–8885, https://doi.org/10.1002/2016JD025213.

Beckman, P., R. Sankaran, C. Catlett, N. Ferrier, R. Jacob, and M. Papka, 2016: Waggle: An open sensor platform for edge computing. *2016 IEEE Sensors*, IEEE, 1–3.

Belcher, S. E., 1999: Wave growth by non-separated sheltering. *European Journal of Mechanics-B/Fluids*, **18 (3)**, 447–462.

Benjamin, S. G., J. M. Brown, G. Brunet, P. Lynch, K. Saito, and T. W. Schlatter, 2018: 100 years of progress in forecasting and nwp applications. *Meteorological Monographs*, **59**, 13.1 – 13.67, https://doi.org/10.1175/AMSMONOGRAPHS-D-18-0020.1.

Berg, L. K., 2016: Two-column aerosol project (TCAP) field campaign report. Technical Report DOE/SC-ARM–16-032, DOE Office of Science Atmospheric Radiation Measurement (ARM) User Facility. https://doi.org/10.2172/1254831.

Berg, L. K., R. K. Newsom, and D. D. Turner, 2017: Year-long vertical velocity statistics derived from Doppler lidar data for the continental convective boundary layer. *Journal of Applied Meteorology and Climatology*, **56 (9)**, 2441–2454.

Bidlot, J.-R., and P. A. Janssen, 2024: Ocean-wave-related changes in the next model upgrade. *ECMWF Newsletter*, **(179)**, 18–25, https://doi.org/10.21957/jb9py41a6f.

Bigorre, S. P., J. B. Edson, R. A. Weller, and J. D. Ware, 2013: A surface mooring for air–sea interaction research in the Gulf Stream. part ii: Analysis of the observations and their accuracies. *Journal of Atmospheric and Oceanic Technology*, **30**, 450–469, https://doi.org/10.1175/JTECH-D-12-00078.1.

Blumberg, W., T. Wagner, D. Turner, and J. Correia Jr, 2017: Quantifying the accuracy and uncertainty of diurnal thermodynamic profiles and convection indices derived from the atmospheric

Accepted for publication in *Bulletin of the American Meteorological Society*. DOI 10.1175/BAMS-D-25-0201.1.

emitted radiance interferometer. *Journal of Applied Meteorology and Climatology*, **56 (10)**, 2747–2766.

Bodini, N., J. K. Lundquist, and A. Kirincich, 2019a: U.S. East coast wind turbines will encounter very low turbulence. *Geophysical Research Letters*, **46 (10)**, 5582–5591.

Bodini, N., J. K. Lundquist, R. Krishnamurthy, M. Pekour, L. K. Berg, and A. Choukulkar, 2019b: Spatial and temporal variability of turbulence dissipation rate in complex terrain. *Atmospheric Chemistry and Physics*, **19 (7)**, 4367–4382.

Bodini, N., and Coauthors, 2024: Wind Data Hub: Event Log / Raw Data. URL https://doi.org/10.21947/3010982, accessed: December 30, 2025, Maintained by Wind Data Hub for U.S. Department of Energy, Office of Energy Efficiency and Renewable Energy, https://doi.org/10.21947/3010982.

Bodini, N., and Coauthors, 2025: Observations of offshore low-level jets off the U.S. East Coast reveal systematic biases in ERA5 and HRRR. *Geophysical Research Letters*, **Under review**.

Bodini, N., and Coauthors, 2026: Nineteen months of daily weather logging on the U.S. East Coast: the WFIP3 event log. *Wind Energy Science*, https://doi.org/10.5194/egusphere-2026-17.

Bourassa, M. A., T. Meissner, I. Cerovecki, P. S. Chang, X. Dong, G. De Chiara, C. Donlon, and Coauthors, 2019: Remotely sensed winds and wind stresses for marine forecasting and ocean modeling. *Frontiers in Marine Science*, **6**, 443, https://doi.org/10.3389/fmars.2019.00443.

Brotzge, J., and Coauthors, 2023: Challenges and opportunities in numerical weather prediction. *Bulletin of the American Meteorological Society*, **104 (3)**, E698–E705, https://doi.org/10.1175/BAMS-D-22-0210.1.

Buckley, M. P., J. Horstmann, I. Savelyev, and J. R. Carpenter, 2025: Direct observations of airflow separation over ocean surface waves. *Nature Communications*, **16 (1)**, 5526.

Chang, Y., S. Zippel, and A. Kirincich, 2025: Shear-flow instability of wind-wave coupling: numerical solutions and field validation. *J. Physical Oceanography*, **submitted**.

Accepted for publication in *Bulletin of the American Meteorological Society.* DOI 10.1175/BAMS-D-25-0201.1.

Cinquino, E., and A. Kirincich, 2024: Whoi metocean data initiative. Technical Report WHOI_MetOcean_2024, Woods Hole Oceanographic Institution. https://doi.org/10.26025/1912/27014.

Clary, J., L. P. Nadeau, and C. Chavanne, 2019: The effect of measurement limitations on high-frequency radar-derived spectral energy fluxes. *Journal of Atmospheric and Oceanic Technology*, **36 (11)**, 2139–2152, https://doi.org/10.1175/JTECH-D-18-0237.1.

Clayson, C. A., C. DeMott, S. de Szoeke, P. Chang, G. R. Foltz, R. Krishnamurthy, T. Lee, and Coauthors, 2023: A new paradigm for observing and modeling of air-sea interactions to advance earth system prediction: A US CLIVAR report. Tech. rep., NCAR.

Colbo, K., and R. A. Weller, 2009: Accuracy of the IMET sensor package in the subtropics. *Journal of Atmospheric and Oceanic Technology*, **26**, 1867–1890.

de Jong, E., E. Quon, and S. Yellapantula, 2023: Mechanisms of low-level jet formation in the U.S. mid-Atlantic offshore. *Journal of the Atmospheric Sciences*, **81**, 31–52, https://doi.org/10.1175/JAS-D-23-0079.1.

De Jong, E., E. Quon, and S. Yellapantula, 2024: Mechanisms of low-level jet formation in the U.S. Mid-Atlantic offshore. *Journal of the Atmospheric Sciences*, **81 (1)**, 31–52.

Debnath, M., P. Doubrawa, M. Optis, P. Hawbecker, and N. Bodini, 2021: Extreme wind shear events in U.S. offshore wind energy areas and the role of induced stratification. *Wind Energy Science*, **6 (4)**, 1043–1059, https://doi.org/10.5194/wes-6-1043-2021.

Dowell, D. C., and Coauthors, 2022: The High-Resolution Rapid Refresh (HRRR): An hourly updating convection-allowing forecast model. part i: Motivation and system description. *Weather and Forecasting*, **37 (8)**, 1371–1395.

Edson, J. B., and Coauthors, 2007: The coupled boundary layers and air-sea transfer experiment in low winds. *Bulletin of the American Meteorological Society*, **88**, 341–356.

Edson, J. B., and Coauthors, 2013: On the exchange of momentum over the ocean. *Journal of Physical Oceanography*, **43 (8)**, 1589–1610.

Accepted for publication in *Bulletin of the American Meteorological Society.* DOI 10.1175/BAMS-D-25-0201.1.

Fairall, C. W., E. F. Bradley, J. E. Hare, A. A. Grachev, and J. B. Edson, 2003: Bulk parameterization of air–sea fluxes: Updates and verification for the COARE algorithm. *Journal of Climate*, **16 (4)**, 571–591.

Farrar, J. T., J. B. Edson, R. W. Schmitt, and Coauthors, 2015: Salinity and temperature balances at the SPURS central mooring during fall and winter. *Oceanography*, **28 (1)**, 56–65.

Farrar, J. T., C. J. Zappa, R. A. Weller, and A. T. Jessup, 2007: Sea surface temperature signatures of oceanic internal waves in low winds. *Journal of Geophysical Research*, **112 (C6)**, C06 014, https://doi.org/10.1029/2006JC003889.

Fovell, R. G., and S. B. Capps, 2024: Sustained wind forecasts from the high-resolution rapid refresh model: skill assessment and bias mitigation. *Atmosphere*, **16 (1)**, 16, https://doi.org/10.3390/atmos16010016.

Fovell, R. G., and A. Gallagher, 2022: An evaluation of surface wind and gust forecasts from the high-resolution rapid refresh model. *Weather and Forecasting*, **37 (6)**, 1049–1068, https://doi.org/10.1175/WAF-D-21-0176.1.

Gaudet, B. J., G. García Medina, R. Krishnamurthy, W. J. Shaw, L. M. Sheridan, Z. Yang, R. K. Newsom, and M. Pekour, 2022: Evaluation of coupled wind–wave model simulations of offshore winds in the Mid-Atlantic bight using lidar-equipped buoys. *Monthly Weather Review*, **150 (6)**, 1377–1395.

Gebauer, J. G., and T. M. Bell, 2024: A flexible, multi-instrument optimal estimation retrieval for wind profiles. *Journal of Atmospheric and Oceanic Technology*, **41 (6)**, 605–620.

Hong, X., S. Lentz, J. B. Edson, and R. A. Weller, 2009: High SST variability south of Martha's Vineyard. *Journal of Marine Systems*, **78 (1)**, 59–76.

Huang, Y., B. J. Gaudet, S. Tai, S. Feng, Z. Yang, and R. Krishnamurthy, 2025: Assessing the influence of ocean-wind-wave coupling on marine boundary layer wind dynamics. *Monthly Weather Review*.

Jackson, R. C., B. A. Raut, D. Dematties, S. M. Collis, N. Ferrier, P. Beckman, and R. Newsom, 2023: ARMing the Edge: Designing Edge Computing-Capable Machine Learning Algorithms

Accepted for publication in *Bulletin of the American Meteorological Society.* DOI 10.1175/BAMS-D-25-0201.1.

to Target ARM Doppler Lidar Processing. *Artificial Intelligence for the Earth Systems*, **2 (4)**, 220 062.

James, E. P., and Coauthors, 2022: The high-resolution rapid refresh (hrrr): an hourly updating convection-allowing forecast model. part ii: Forecast performance. *Weather and Forecasting*, **37 (8)**, 1397–1417.

Janssen, P. A., 1991: Quasi-linear theory of wind-wave generation applied to wave forecasting. *Journal of Physical Oceanography*, **21 (11)**, 1631–1642.

Jeffreys, H., 1925: On the formation of water waves by wind. *Proceedings of the Royal Society of London. Series A*, **107 (742)**, 189–206.

Jiang, H., 2026: Evaluation of planetary boundary-layer schemes in the WRF model for modeling low-level winds in the marine atmospheric boundary layer: case studies of various boundary-layer types. *in prep.*

Jiang, H., and J. B. Edson, 2020: Characterizing marine atmospheric boundary layer to support offshore wind energy research. *Journal of Physics: Conference Series*, IOP Publishing, Vol. 1452, 012027.

Juliano, T., B. Kosović, P. A. Jimenez, M. Eghdami, S. E. Haupt, and A. Martilli, 2022: "gray zone" simulations using a three-dimensional planetary boundary layer parameterization in the Weather Research and Forecasting model. *Monthly Weather Review*, **150 (7)**, 1585–1619.

Kim, S. Y., E. Terrill, and B. Cornuelle, 2007: Objectively mapping HF radar-derived surface current data using measured and idealized data covariance matrices. *J. Geophys. Res.*, **112 (C06021)**, doi:10.1029/2006JC003 756.

Kirincich, A., and B. Emery, 2023: Revisiting HF ground wave propagation losses over the ocean: A comparison of long-term observations and models. *Radio Science*, **58 (4)**, 1–24.

Kirincich, A., and B. Emery, 2026: Mapping coastal ocean surface winds with high-frequency radar: A tomographic approach. *Journal of Atmospheric and Oceanic Technology*, **43 (5)**, 637–654.

Accepted for publication in *Bulletin of the American Meteorological Society.* DOI 10.1175/BAMS-D-25-0201.1.

Kirincich, A., B. Emery, L. Washburn, and P. Flament, 2019: Improving surface current resolution using direction finding algorithms for multiantenna high-frequency radars. *Journal of Atmospheric and Oceanic Technology*, **36 (10)**, 1997–2014.

Kirincich, A., B. Hodges, P. Flament, and V. Futch, 2022: Horizontal stirring over the Northeast U.S. Continental shelf: The spatial and temporal evolution of surface eddy kinetic energy. *Journal of Geophysical Research: Oceans*, **127**, 1–22, https://doi.org/10.1029/2021jc017307.

Kosović, B., and Coauthors, 2020: Three-dimensional planetary boundary layer parameterization for high-resolution mesoscale simulations. *Journal of Physics: Conference Series*, Vol. 1452.

Krishnamurthy, R., A. Choukulkar, R. Calhoun, J. Fine, A. Oliver, and K. S. Barr, 2013: Coherent Doppler lidar for wind farm characterization. *Wind Energy*, **16 (2)**, 189–206.

Krishnamurthy, R., A. Kirincich, and D. Turner, 2025: Wind Forecasting Improvement Project 3 (WFIP-3): Project Dataset. URL https://doi.org/10.21947/WFIP3/3008589, Wind Data Hub funded by U.S. Department of Energy, Office of Energy Efficiency and Renewable Energy's Wind Energy Technologies Office operated and maintained by Pacific Northwest National Laboratory, https://doi.org/10.21947/WFIP3/3008589.

Krishnamurthy, R., and Coauthors, 2023: Year-long buoy-based observations of the air–sea transition zone off the us west coast. *Earth System Science Data*, **15**, 5667–5699, https://doi.org/10.5194/essd-15-5667-2023.

Lentz, S., S. Elgar, and R. Guza, 2003: Observations of the flow field near the nose of a buoyant coastal current. *Journal of Physical Oceanography*, **33 (4)**, 933–943.

Lentz, S. J., 2008: Seasonal variations in the circulation over the Middle Atlantic Bight continental shelf. *Journal of Physical Oceanography*, **38 (7)**, 1486–1500, https://doi.org/10.1175/2007JPO3767.1.

Lombardo, K., and B. A. Colle, 2013: Processes controlling the structure of two convective systems crossing the southern New England coast. *Monthly Weather Review*, **141**, 3710–3734.

Lombardo, K., B. A. Colle, J. Edson, and Coauthors, 2016: Sensitivity of simulated sea breezes to initial conditions in complex coastal regions. *Monthly Weather Review*, **144 (4)**, 1299–1320.

Accepted for publication in *Bulletin of the American Meteorological Society*. DOI 10.1175/BAMS-D-25-0201.1.

Lombardo, K., and T. Kading, 2018: The behavior of squall lines in horizontally heterogeneous coastal environments. *Journal of the Atmospheric Sciences*, **75 (4)**, 1243–1269.

Lombardo, K. A., and B. A. Colle, 2012: Ambient conditions associated with the maintenance and decay of quasi-linear convective systems crossing the NE U.S. coast. *Monthly Weather Review*, **140**, 3805–3819.

Mahrt, L., J. B. Edson, I. Vickers, and L. A., 2014: Low-level wind maxima and structure of the stably stratified boundary layer in the coastal zone. *Journal of Applied Meteorology and Climatology*, **53 (2)**, 363–376.

Marcial, D., and Coauthors, 2024: Evaluation of an automated eddy covariance air-sea flux package on a floating lidar buoy. Session: Atmospheric Sciences / Observational and Modeling Studies for Improved Wind Energy Characterization and Forecasting III Poster, Poster No. 1795, id. A41O-1795, AGU Fall Meeting 2024, Washington, D.C., 9-13 December 2024.

McCabe, E. J., and J. M. Freedman, 2023: Development of an objective methodology for identifying the sea-breeze circulation and associated low-level jet in the New York Bight. *Weather and Forecasting*, **38 (4)**, 571–589, https://doi.org/10.1175/WAF-D-22-0173.1.

Michaud-Belleau, V., M. Gaudreau, J. Lacoursière, E. Boisvert, L. Ravelomanantsoa, D. D. Turner, and L. Rochette, 2025: The atmospheric sounder spectrometer by infrared spectral technology (ASSIST): instrument design and signal processing. *Atmospheric Measurement Techniques*, **18 (14)**, 3585–3609, https://doi.org/10.5194/amt-18-3585-2025.

Miles, J. W., 1957: On the generation of surface waves by shear flows. *Journal of Fluid Mechanics*, **3 (2)**, 185–204.

National Research Council, 1997: *Boundary Layer Dynamics*. National Academies Press, https://doi.org/10.17226/5710.

National Research Council, 2018: *Future of atmospheric boundary layer observing, understanding, and modeling*. NATIONAL ACADEMIES Press, 48 pp.

Newsom, R. K., W. A. Brewer, J. M. Wilczak, D. E. Wolfe, S. P. Oncley, and J. K. Lundquist, 2017: Validating precision estimates in horizontal wind measurements from a

Accepted for publication in *Bulletin of the American Meteorological Society*. DOI 10.1175/BAMS-D-25-0201.1.

Doppler lidar. *Atmospheric Measurement Techniques*, **10 (3)**, 1229–1240, https://doi.org/10.5194/amt-10-1229-2017.

Newsom, R. K., and R. Krishnamurthy, 2022: Doppler lidar (DL) instrument handbook. Technical Report DOE/SC-ARM/TR-101, DOE Office of Science Atmospheric Radiation Measurement (ARM) User Facility.

Nonaka, M., and S.-P. Xie, 2003: Covariations of sea surface temperature and wind over the Kuroshio and its extension: Evidence for ocean-to-atmosphere feedback. *Journal of Climate*, **16 (9)**, 1404–1413.

Olson, J. B., J. S. Kenyon, W. Angevine, J. M. Brown, M. Pagowski, and K. Sušelj, 2019a: A description of the MYNN-EDMF scheme and the coupling to other components in WRF–ARW. Tech. rep., NOAA Technical Memorandum. https://doi.org/https://doi.org/10.25923/n9wm-be49.

Olson, J. B., and Coauthors, 2019b: Improving wind energy forecasting through numerical weather prediction model development. *Bulletin of the American Meteorological Society*, **100 (11)**, 2201–2220.

Olson, J. B., and Coauthors, 2026: A description of the MYNN-EDMF turbulence scheme. NOAA Technical Memorandum GSL-77, National Oceanic and Atmospheric Administration, Oceanic and Atmospheric Research, Global Systems Laboratory. https://doi.org/10.25923/rahr-sj70.

O'Connor, E. J., A. J. Illingworth, I. M. Brooks, C. D. Westbrook, R. J. Hogan, F. Davies, and B. J. Brooks, 2010: A method for estimating the turbulent kinetic energy dissipation rate from a vertically pointing Doppler lidar, and independent evaluation from balloon-borne in situ measurements. *Journal of atmospheric and oceanic technology*, **27 (10)**, 1652–1664.

Piazza, M., L. Terray, J. Boé, E. Maisonnave, and E. Sanchez-Gomez, 2016: Influence of small-scale North Atlantic sea surface temperature patterns on the marine boundary layer and free troposphere: A study using the atmospheric ARPEGE model. *Climate Dynamics*, **46**, 1699–1717.

Accepted for publication in *Bulletin of the American Meteorological Society*. DOI 10.1175/BAMS-D-25-0201.1.

Pichugina, Y. L., and Coauthors, 2017: Properties of the offshore low level jet and rotor layer wind shear as measured by scanning Doppler lidar: Offshore low level jet from scanning Doppler lidar measurements. *Wind Energy*, **20 (6)**, 987–1002, https://doi.org/10.1002/we.2075.

Quint, D., J. K. Lundquist, and D. Rosencrans, 2025: Simulations suggest offshore wind farms modify low-level jets. *Wind Energy Science*, **10 (1)**, 117–142, https://doi.org/10.5194/wes-10-117-2025.

Sauvage, C., H. Seo, C. A. Clayson, and J. B. Edson, 2023: Improving Wave-Based Air-Sea Momentum Flux Parameterization in Mixed Seas. *Journal of Geophysical Research: Oceans*, **128 (3)**, e2022JC019 277, https://doi.org/10.1029/2022JC019277.

Sauvage, C., H. Seo, S. Zippel, C. A. Clayson, and J. B. Edson, 2025: Fetch-dependent surface wave responses to offshore wind farms in the Northeast U.S. coast. **130 (12)**, e2025JC023 156, https://doi.org/10.1029/2025JC023156.

Schlundt, M., J. T. Farrar, S. P. Bigorre, A. J. Plueddemann, and R. A. Weller, 2020: Accuracy of wind observations from open-ocean buoys: Correction for flow distortion. *Journal of Atmospheric and Oceanic Technology*, **37 (4)**, 687–703.

Seo, H., A. Miller, and J. Roads, 2007: The Scripps coupled ocean-atmosphere regional (scoar) model. *Journal of Climate*, **20 (3)**, 381–402.

Seo, H., C. Sauvage, C. Renkl, J. K. Lundquist, and A. Kirincich, 2025: Sea surface warming and ocean-to-atmosphere feedback driven by large-scale offshore wind farms under seasonally stratified conditions. *Science Advances*, **11 (45)**, eadw7603, https://doi.org/10.1126/sciadv.adw7603.

Shaw, W., and Coauthors, 2022: Scientific challenges to characterizing the wind resource in the marine atmospheric boundary layer. *Wind Energy Science*, **(6)**, 2307–2334, https://doi.org/10.5194/wes-7-2307-2022.

Shaw, W. J., and Coauthors, 2019: The second wind forecast improvement project (WFIP2): General overview. *Bulletin of the American Meteorological Society*, **100**, 1687–1699, https://doi.org/10.1175/BAMS-D-18-0036.1.

Accepted for publication in *Bulletin of the American Meteorological Society.* DOI 10.1175/BAMS-D-25-0201.1.

Shearman, R. K., and S. J. Lentz, 2010: Long-term sea surface temperature variability along the U.S. East Coast. *Journal of Physical Oceanography*, **40 (5)**, 1004–1017, https://doi.org/10.1175/2009jpo4300.1.

Sheridan, L. M., R. Krishnamurthy, W. I. Gustafson Jr, Y. Liu, B. J. Gaudet, N. Bodini, R. K. Newsom, and M. Pekour, 2023: Offshore low-level jet observations and model representation using lidar buoy data off the California coast. *Wind Energy Science Discussions*, **2023**, 1–28.

Shutt, M., and H. Seim, 2020: Assessment of stability-based characterizations of North Carolina's offshore wind resource using a nested boundary layer method. *J. Energy Power Tech.*, **2**, 006, https://doi.org/10.21926/jept.2002006.

Skyllingstad, E. D., and J. B. Edson, 2009: Large-eddy simulation of moist convection during a cold air outbreak over the Gulf Stream. *Journal of the Atmospheric Sciences*, **66 (5)**, 1274–1293.

Solheim, F., J. R. Godwin, E. Westwater, Y. Han, S. J. Keihm, K. Marsh, and R. Ware, 1998: Radiometric profiling of temperature, water vapor and cloud liquid water using various inversion methods. *Radio Science*, **33 (2)**, 393–404.

Sorooshian, A., A. F. Corral, R. A. Braun, B. Cairns, E. Crosbie, and e. a. Ferrare, R., 2020: Atmospheric research over the western North Atlantic ocean region and North American east coast: A review of past work and challenges ahead. *Journal of Geophysical Research: Atmospheres,*, **125**, 29–49, https://doi.org/10.1029/2019JD031626.

Stull, R. B., 1988: *An Introduction to Boundary Layer Meteorology*. 1st ed., Atmospheric Sciences Library, Kluwer Academic Publishers, Dordrecht, The Netherlands.

Sullivan, P. P., J. B. Edson, J. B. Edson, M. L., and T. F., 2008: Large-eddy simulations atmospheric marine boundary layers above nonequilibrium surface waves. *Journal of the Atmospheric Sciences*, **65 (4)**, 1225–1245.

Sullivan, P. P., J. C. McWilliams, and E. G. Patton, 2025: An investigation of coupled atmospheric and oceanic boundary layers using large-eddy simulation. *Journal of the Atmospheric Sciences*, **82 (4)**, 829–846.

Tai, S.-L., B. Gaudet, S. Feng, R. Krishnamurthy, L. K. Berg, and J. D. Fast, 2025: Characterizing model uncertainties in simulated coast-to-offshore wind over the Northeast U.S. using

Accepted for publication in *Bulletin of the American Meteorological Society*. DOI 10.1175/BAMS-D-25-0201.1.

multi-platform measurements from the TCAP field campaign. *Renewable Energy*, **239**, 122 022, https://doi.org/10.1016/j.renene.2025.122022.

Timpe, G., and N. Van de Voorde, 1995: NOMAD buoys: an overview of forty years of use. *'Challenges of Our Changing Global Environment'. Conference Proceedings. OCEANS'95 MTS/IEEE*, IEEE, Vol. 1, 309–315.

Turner, D. D., and W. G. Blumberg, 2019: Improvements to the AERIoe thermodynamic profile retrieval algorithm. *IEEE Journal of Selected Topics in Applied Earth Observations and Remote Sensing*, **12 (5)**, 1339–1354.

Turner, D. D., H. Cutler, M. Shields, R. Hill, B. Hartman, Y. Hu, T. Lu, and H. Jeon, 2022: Evaluating the economic impacts of improvements to the high-resolution rapid refresh (hrrr) numerical weather prediction model. *Bulletin of the American Meteorological Society*, **103 (2)**, E198–E211.

Turner, D. D., and U. Löhnert, 2014: Information content and uncertainties in temperature and humidity profiles from the ground-based atmospheric emitted radiance interferometer (AERI). *Journal of Applied Meteorology and Climatology*, **53 (3)**, 752–771.

Turner, D. D., and U. Löhnert, 2021: Ground-based temperature and humidity profiling: combining active and passive remote sensors. *Atmos. Meas. Tech.*, **14**, 3033–3048, https://doi.org/10.5194/amt-14-3033-2021.

Wang, Q., and Coauthors, 2018: CASPER: Coupled air–sea processes and electromagnetic ducting research. *B. Am. Meteorol. Soc.*, **99**, 1449–1471, https://doi.org/10.1175/bams-d-16-0046.1.

Warner, J. C., B. Armstrong, R. He, and J. B. Zambon, 2010: Development of a Coupled Ocean–Atmosphere–Wave–Sediment Transport (COAWST) Modeling System. *Ocean Modelling*, **35 (3)**, 230–244, https://doi.org/10.1016/j.ocemod.2010.07.010.

Wenegrat, J. O., and R. S. Arthur, 2018: Response of the atmospheric boundary layer to submesoscale sea surface temperature fronts. *Geophysical Research Letters*, **45**, 13 505–13 512, https://doi.org/10.1029/2018GL081034.

Accepted for publication in *Bulletin of the American Meteorological Society.* DOI 10.1175/BAMS-D-25-0201.1.

Wilczak, J., and Coauthors, 2015: The wind forecast improvement project (WFIP): A public–private partnership addressing wind energy forecast needs. *Bulletin of the American Meteorological Society*, **96 (10)**, 1699–1718.

Wilczak, J. M., and Coauthors, 2019: The second wind forecast improvement project (WFIP2): Observational field campaign. *Bulletin of the American Meteorological Society*, **100**, 1701–1723, https://doi.org/10.1175/BAMS-D-18-0035.1.

Wilkin, J., 2006: The summertime heat budget and circulation of southeast New England shelf waters. *Journal of Physical Oceanography*, **36**, 1997–2011.

Wood, R., 2012: Stratocumulus clouds. *Monthly Weather Review*, **140 (8)**, 2373 – 2423, https://doi.org/10.1175/MWR-D-11-00121.1.

Xia, G., C. Draxl, M. Optis, and S. Redfern, 2021: Detecting and characterizing sea breezes over the U.S. Northeast coast with implication for offshore wind energy. *Wind Energy Science Discussions*, **2021**, 1–23.

Zhang, X., J.-W. Bao, B. Chen, and E. D. Grell, 2018: A three-dimensional scale-adaptive turbulent kinetic energy scheme in the WRF-ARW model. *Monthly Weather Review*, **146**, 2023–2045.

Zippel, S. F., J. B. Edson, M. E. Scully, and O. R. Keefe, 2024: Direct observation of wave-coherent pressure work in the atmospheric boundary layer. *Journal of Physical Oceanography*, **54 (2)**, 445–459.

Zuidema, P., G. Torri, C. Muller, and A. Chandra, 2017: A survey of precipitation-induced atmospheric cold pools over oceans and their interactions with the larger-scale environment. *Surveys in Geophysics*, **38 (6)**, 1283–1305.

Accepted for publication in *Bulletin of the American Meteorological Society*. DOI 10.1175/BAMS-D-25-0201.1.